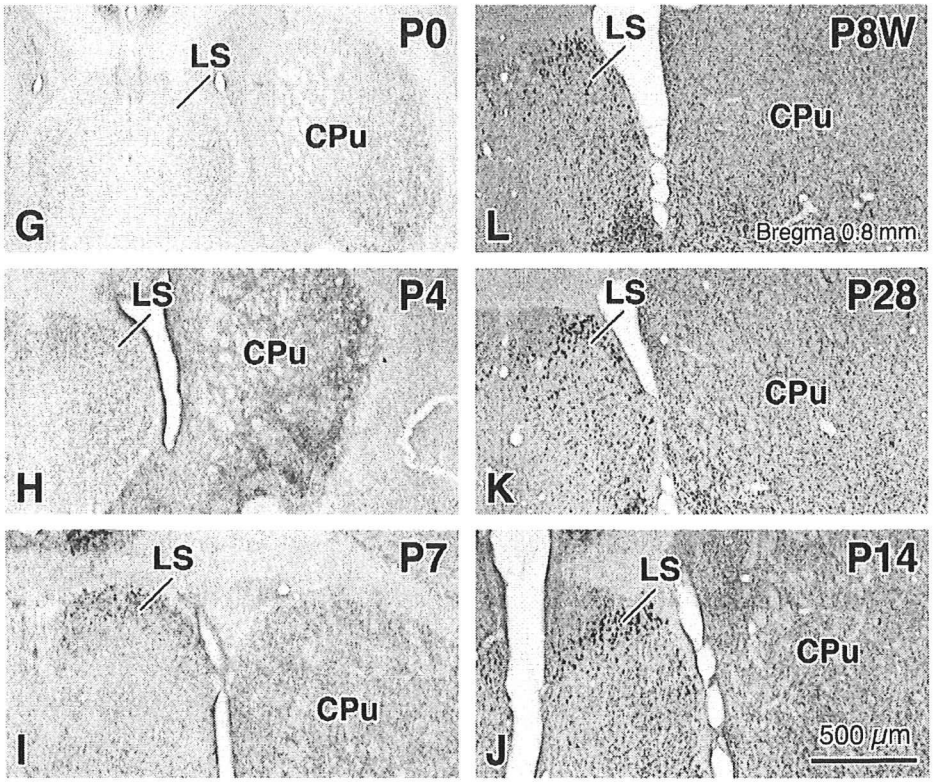

Fig. 3. (*Continued*).

the type 2a pattern was seen in the lateral subdivision (7NL), whereas the type 1b pattern was observed in the medial subdivision (7NM) (Fig. 4G–L; Table 1). In type 2b, weak *Wfs1* mRNA signals were constantly seen at each of the postnatal stages. This pattern was observed in the main olfactory bulb (MOB), the accessory olfactory bulb (AOB), the supraoptic nucleus (SO), the magnocellular part of the paraventricular hypothalamic nucleus (PVNm), the inferior colliculus (IC), nucleus coeruleus (LC), the dorsal raphe nucleus, the median raphe nucleus, the cochlear nucleus (Co), the brainstem reticular formation, and in the Purkinje cell layer of the cerebellar cortex (Figs. 1 and 5A–F; Table 1).

In the type 3 pattern, *Wfs1* mRNA signals peaked from P7 to P14. Type 3 was also categorized into two subtypes (3a and 3b) according to the strength of *Wfs1* mRNA expression at its peak. In type 3a, moderate *Wfs1* mRNA signals were seen from P7 to P14, while weak signals were observed at both P0–P4 and P28–early adulthood (P8W). This pattern was observed in the thalamic reticular nucleus (Rt) (Figs. 1, 5G–L; Table 1). In type 3b, weak *Wfs1* mRNA signals were seen from P7 to P14. This pattern was observed in layer V of the cerebral cortices: the motor (MoCV), somatosensory (SoCV), auditory (AuCV), visual (ViCV), cingulate (CgV), and retrosplenial (RSCV) cortices (Figs. 1, 3A–F; Table 1). It was also seen in layer II of the retrosplenial cortex (RSCII) (Table 1).

3.2. Strong *Wfs1* mRNA expression in the CA1 field, parasubiculum (PaS), and entorhinal cortex in early adulthood

As described in the preceding section, the most intense *Wfs1* mRNA signals were observed in the CA1 field, the PaS, and in the entorhinal cortex (MEA and LEA) from P14 to early adulthood (P8W). To examine cell-specific *Wfs1* mRNA expression, we made a detailed analysis of the distribution of *Wfs1* mRNA signals in these cortical areas of the young-adult mouse (P8W) as a preliminary account of a future analysis of the entire mouse brain structure. Because definitions of areal demarcation and laminar classification are necessary for the interpretation of the experimental results, we will briefly describe our criteria for determining the border of the cortical area and those of the cortical layer before describing the distribution of *Wfs1* mRNA signals. In addition, a description of the pertinent cytoarchitectonic features of each cortical area is accompanied by a description of the distribution of *Wfs1* mRNA signals. To represent the distribution of *Wfs1* mRNA signals, we show side by side the features of the distribution and Nissl-stained sections that correspond to the distribution in the figures.

3.2.1. CA1 field

3.2.1.1. Cytoarchitecture. Areal demarcation was based on Witter and Amaral (2004). According to the size of pyramidal cells in the hippocampus proper, the CA1 field was defined as a small-celled distal (closer to the subiculum) region, while the CA2 and CA3 fields were characterized as large-celled proximal (closer to the dentate gyrus) region. In the CA3 field, small Nissl-stained cells were scattered above the pyramidal cell layer (arrows in Fig. 6B), however a few of these cells were seen in the CA1 and CA2 fields (Fig. 6B).

3.2.1.2. Wfs1 mRNA signals. Wfs1 mRNA signals were observed in the pyramidal cell layer. These signals were confined to the CA1 field. Strong signals were observed in the rostro-medial (septal) part of the CA1 field (Fig. 6A), while weak-to-moderate signals were seen in the caudo-lateral (temporal) part (data not shown). In the rostral part of the CA1 field, there was a tendency for *Wfs1* mRNA signals to be stronger in the medial part than in the lateral part (Fig. 6A). In addition to the pyramidal cell layer, weakly-to-moderately *Wfs1* mRNA-hybridized neurons were seen in strata radiatum and oriens (arrows in Fig. 6A and C).

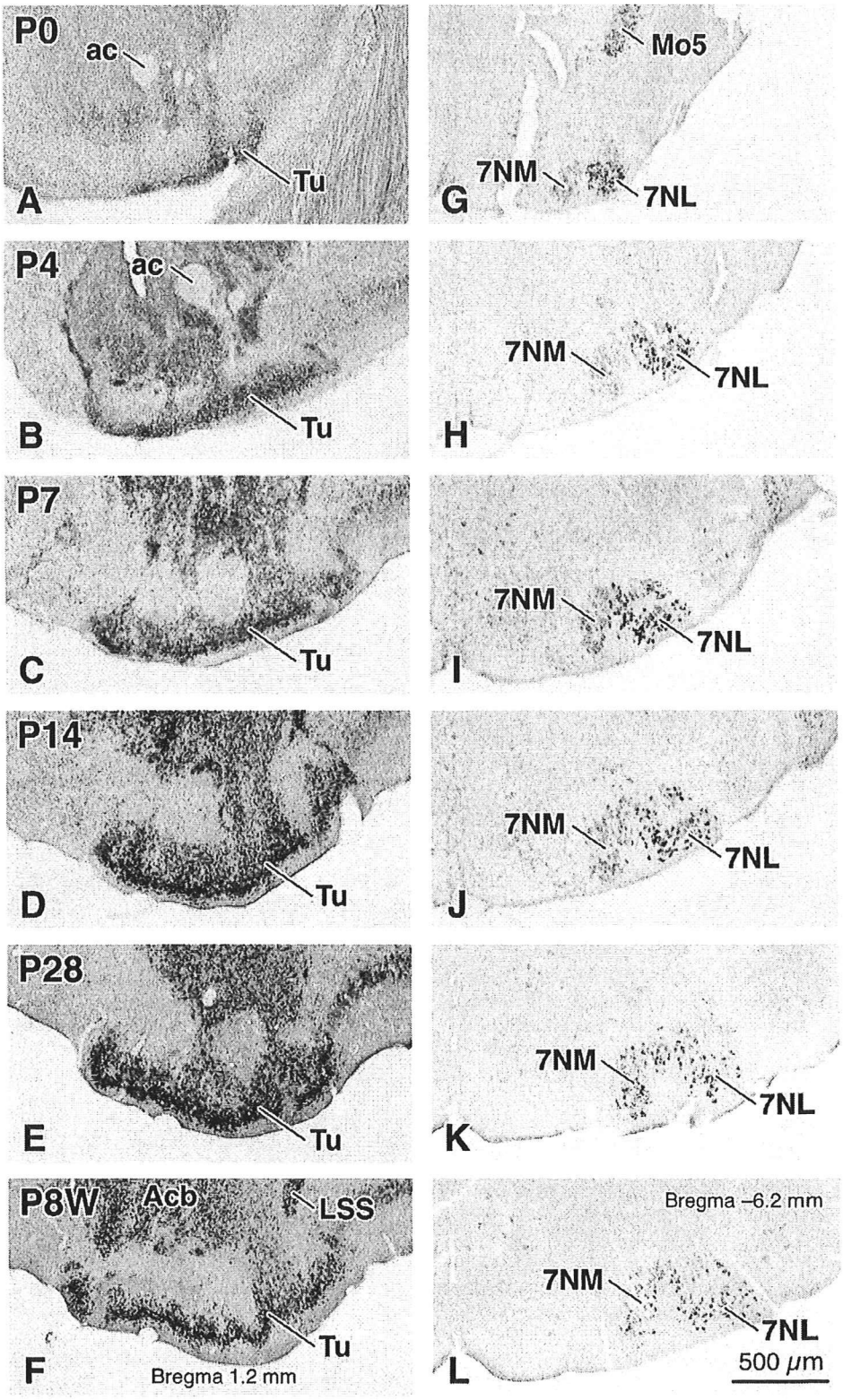

Fig. 4. Type 2a pattern of *Wfs1* mRNA signals in the mouse brain during postnatal development. (A–F) Changes in *Wfs1* mRNA signals in the olfactory tuberculum (Tu) during postnatal development. The day of birth is regarded as postnatal day 0 (P0). P4, P7, P14, P28, and P8W indicate postnatal days 4, 7, 14, and 28, and postnatal week 8, respectively. Brain sections of P0, P4, P7, P14, P28, and of P8W mice are shown in panels (A), (B), (C), (D), (E), and (F), respectively. The bregma level of a P8W-mouse section is represented at the lower middle in (F). (G–L) Changes in *Wfs1* mRNA signals in the facial nucleus during postnatal development. Brain sections of P0, P4, P7, P14, P28, and of P8W mice are shown in panels (G), (H), (I), (J), (K), and (L), respectively. The bregma level of a P8W-mouse section is represented at the upper right in (L). Note that *Wfs1* mRNA signals in the type 2a pattern are moderate, and of a relatively stable strength from P0 to P8W. Additionally, in the facial nucleus, the pattern of *Wfs1* mRNA signals during postnatal development is not homogeneous. In the lateral subdivision of the facial nucleus (7NL), the pattern is type 2a, whereas in the medial subdivision (7NM), it is type 1b. Upper and right sides of each panel are dorsal and lateral sides of each brain section, respectively. ac, anterior commissure; Acb, nucleus accumbens, LSS, lateral stripe of the striatum; Mo5, motor nucleus of the trigeminal nerve. Scale bar = 500 μm in (L) for (A–K).

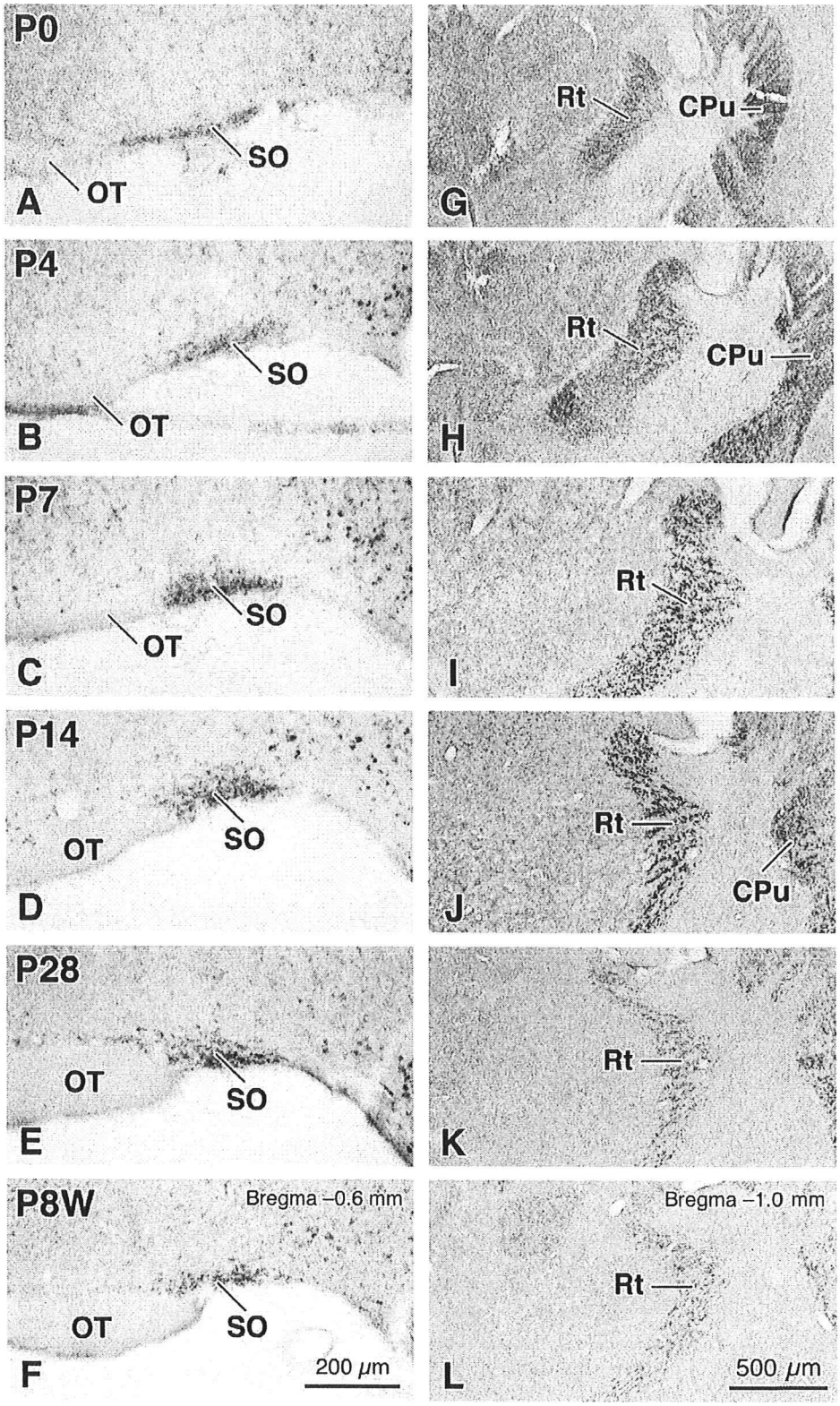

Fig. 5. Type 2b (A–F) and type 3a (G–L) patterns of *Wfs1* mRNA signals in the mouse brain during postnatal development. (A–F) Changes in *Wfs1* mRNA signals in the supraoptic nucleus (SO) during postnatal development. The day of birth is regarded as postnatal day 0 (P0). P4, P7, P14, P28, and P8W indicate postnatal days 4, 7, 14, and 28, and postnatal week 8, respectively. Brain sections of P0, P4, P7, P14, P28, and of P8W mice are shown in panels (A), (B), (C), (D), (E), and (F), respectively. The bregma level of a P8W-mouse section is represented at the upper right in (F). Note that *Wfs1* mRNA signals in the type 2b pattern are weak, and of a relatively stable strength from P0 to P8W. (G–L) Changes in *Wfs1* mRNA signals in the thalamic reticular nucleus (Rt) during postnatal development. Brain sections of P0, P4, P7, P14, P28, and of P8W mice are shown in panels (G), (H), (I), (J), (K), and (L), respectively. The bregma level of a P8W-mouse section is represented at the upper right in (L). Note that *Wfs1* mRNA signals in the type 3a pattern peak from P7 to P14 and show moderate strength at the peak. Upper and right sides of each panel are dorsal and lateral sides of each brain section, respectively. CPu, caudate putamen; OT, optic tract. Scale bar = 200 μm in (F) for (A–E), 500 μm in (L) for (G–K).

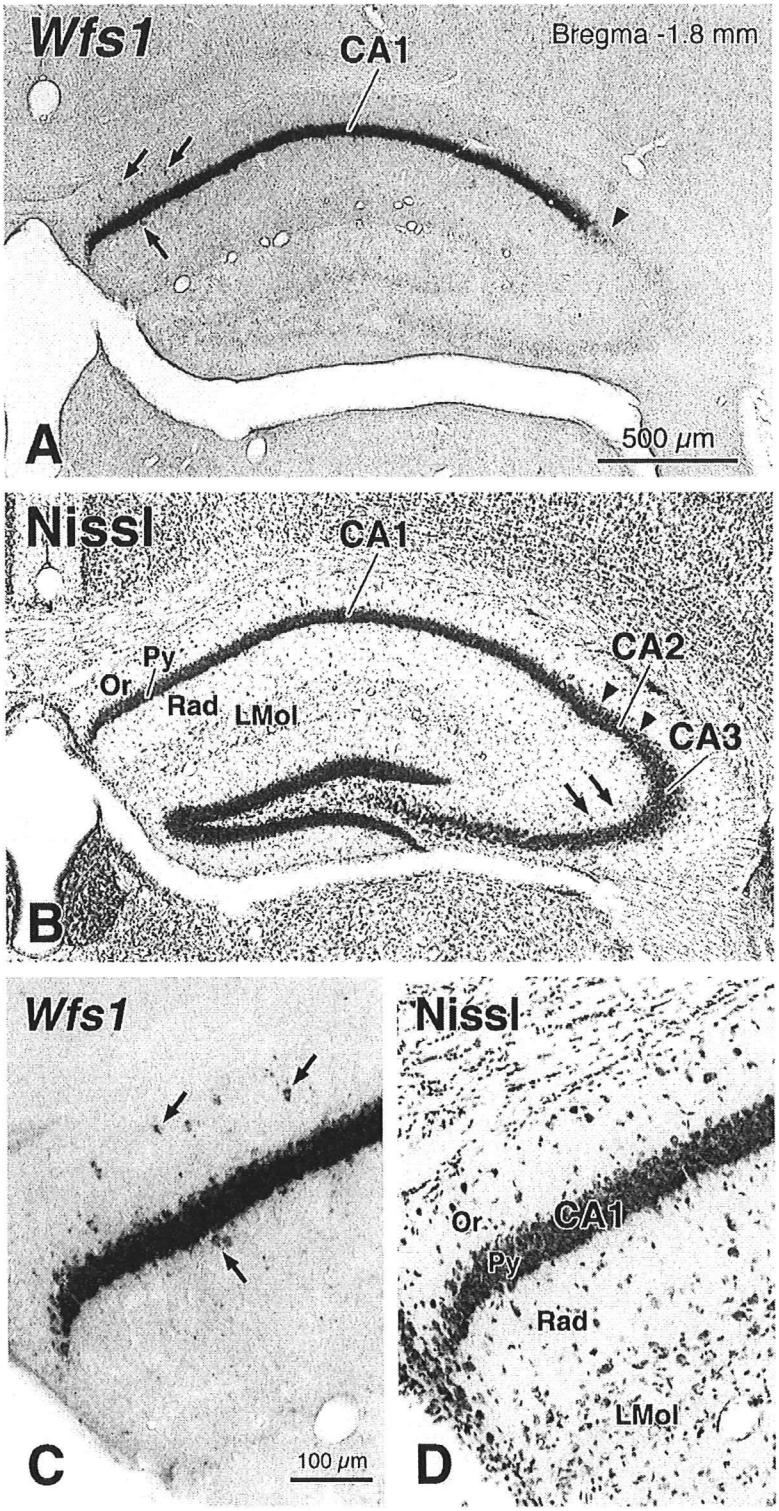

Fig. 6. *Wfs1* mRNA signals in the rostral part (Bregma = −1.8 mm) of the hippocampal formation in the young-adult mouse (postnatal week 8). (A and B) Mouse *Wfs1* mRNA signals (*Wfs1*, A), and cytoarchitecture (Nissl, B) in adjacent sections of the hippocampal formation hybridized with anti-sense cRNA probes of the mouse *Wfs1* 3′-terminus, and Nissl-stained with cresyl violet, respectively. Arrowheads indicate borders between each hippocampal field. Arrows in (A), and those in (B) show *Wfs1* mRNA-hybridized neurons in strata radiatum and oriens of the CA1 field, and small Nissl-stained cells scattered above the pyramidal cell layer of the CA3 field, respectively. (C and D) Higher magnification photomicrographs of mouse *Wfs1* mRNA signals (*Wfs1*, C) in the same section as in panel (A) and of cytoarchitecture (Nissl, D) in the same section as in panel (B). Arrows in (C) show the identical set of *Wfs1* mRNA-hybridized neurons pointed to by arrows in (A). Note that strong *Wfs1* mRNA signals are almost exclusively observed in the pyramidal cell layer of the CA1 field. In addition, *Wfs1* mRNA-hybridized neurons (arrows in A and C) are seen in strata oriens and radiatum of the CA1 field. CA1, CA1 field of the hippocampus; CA2, CA2 field of the hippocampus; CA3, CA3 field of the hippocampus; LMol, stratum lacunosum-moleculare; Or, stratum oriens; Py, pyramidal cell layer; Rad, stratum radiatum. Scale bars = 500 μm in (A) for (B), 100 μm in (C) for (D).

3.2.2. PaS

3.2.2.1. Cytoarchitecture. Areal demarcation and the laminar classification were based on Witter and Amaral (2004). From the cytoarchitectonic aspect, the PaS (Brodmann's area 49) is a multilayered structure in which there are more than three cortical layers. The layers of the PaS are subdivided into external and internal laminae, separated by a cell-free lamina (layer IV). The external lamina is composed of the molecular layer (layer I) and cell layers II and III, and the internal lamina, cell layers V and VI. Layers II and III comprise large, rather densely packed, lightly stained cells. There is no clear boundary between layers II and III of the external lamina. Layers V and VI consist of small, rather densely packed, moderately stained cells (Fig. 7B and D).

3.2.2.2. Wfs1 mRNA signals. Strong *Wfs1* mRNA signals were observed in cell layers II and III (the external lamina except for layer I). In the deep part of the external lamina, weak-to-moderate signals were also seen deeper down (Fig. 7).

3.2.3. Entorhinal cortex

3.2.3.1. Cytoarchitecture. Areal demarcation and the laminar classification were based on Insausti et al. (1997) and on Witter and

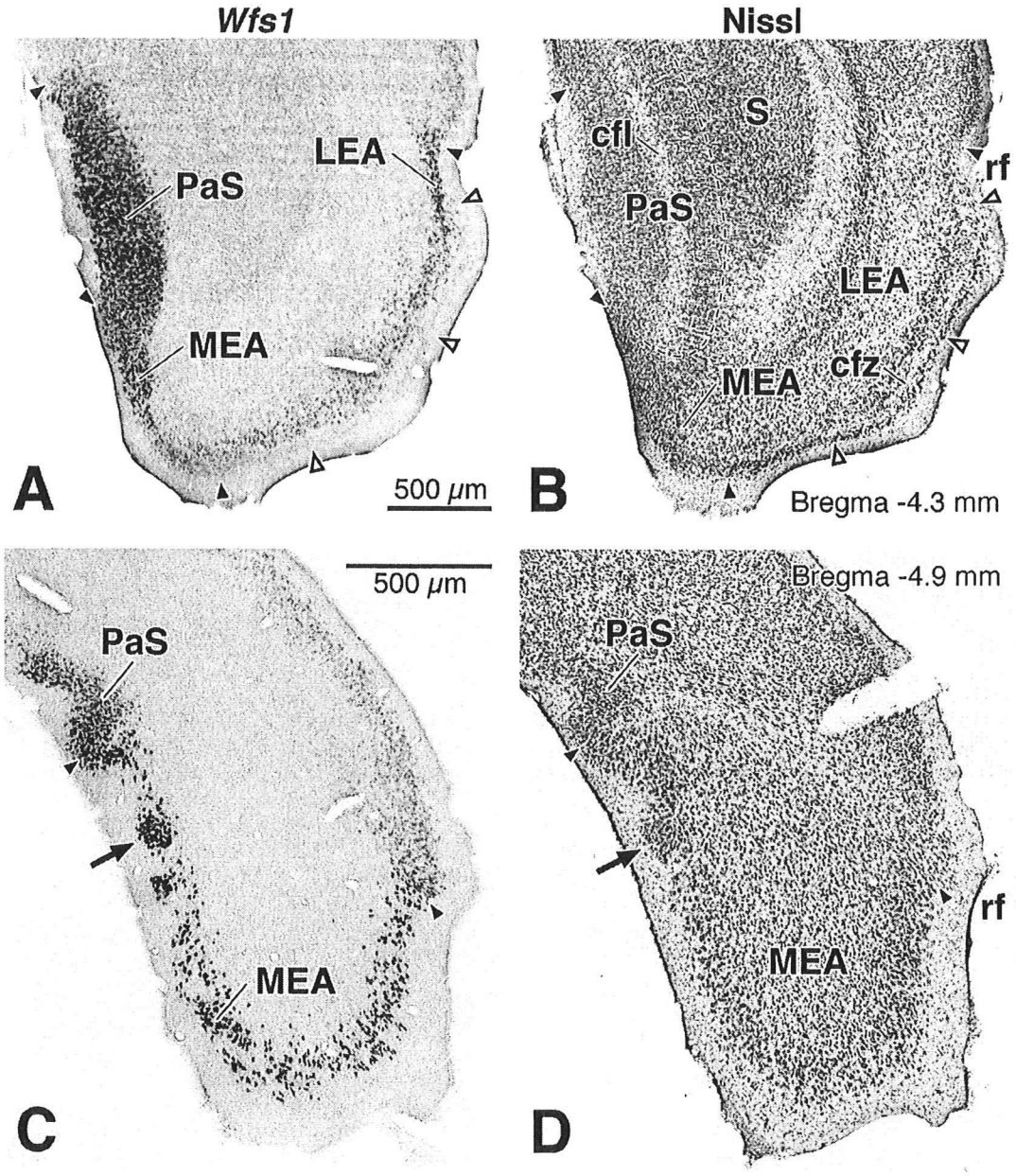

Fig. 7. *Wfs1* mRNA signals in the parasubiculum (PaS) and entorhinal cortex of the young-adult mouse (postnatal week 8). (A and B) Mouse *Wfs1* mRNA signals (*Wfs1*, A), and cytoarchitecture (Nissl, B) in adjacent sections of the rostral part (Bregma = −4.3 mm) hybridized with anti-sense cRNA probes of the mouse *Wfs1* 3′-terminus, and Nissl-stained with cresyl violet, respectively. The dashed line in (B) shows the border of the PaS. (C and D) Mouse *Wfs1* mRNA signals (*Wfs1*, C), and cytoarchitecture (Nissl, D) in adjacent sections of the caudal part (Bregma = −4.9 mm). Solid and open arrowheads indicate borders between each cortical area and the superficial boundary of layer II in the lateral entorhinal area (LEA), respectively. Arrows show an islet of cells in layer II of the medial entorhinal area (MEA). Note that strong *Wfs1* mRNA signals are observed in the PaS, MEA, and LEA. cfl, cell-free lamina; cfz, cell-free zone; rf, rhinal fissure; S, subiculum. Scale bars = 500 μm in (A) for (B), in (C) for (D).

Amaral (2004). In this study, the entorhinal cortex is subdivided into two areas, the MEA and the LEA. In the MEA, cells in layer II are primarily large-to-medium-sized, moderately packed, and moderately stained, while those in layer III are small-to-medium-sized and loosely packed (Fig. 7B and D). In the caudo-medial part of layer II, an islet of cells (arrow in Fig. 7D) was observed. Cells in the islet were medium-sized, rather densely packed, and lightly stained (Fig. 7D). In the rostro-medial part, which abuts the PaS, layer I is very thin and layers II and III contain densely packed cells that are small-to-medium-sized, and moderately stained (Fig. 7B).

In the LEA, layer II is separated from layer III by a narrow cell-free zone in much of the rostral part. Cells in layer II are very densely packed, while those in layer III are moderately or loosely packed. Layer III is thick and subdivided into a narrow moderately packed outer zone and a loosely packed inner zone. Since layer IV is very poorly developed or absent, layer V usually abuts layer III. Cells in layer V tend to be larger and more darkly stained than those in layer III (Fig. 7B).

3.2.3.2. Wfs1 mRNA signals. In the caudal part of the MEA, strong *Wfs1* mRNA signals were observed in layer II. These signals were almost confined to this layer (Fig. 7C and D). In layer II of the caudo-medial part, islets of strongly *Wfs1* mRNA-hybridized cells were seen (arrow in Fig. 7C). One of these islets corresponded to an islet of Nissl-stained cells (arrow in Fig. 7D). Strongly *Wfs1* mRNA-hybridized cells were densely packed in the islets, while those were scattered around the islets (Fig. 7C). In the rostro-medial part of the MEA, strongly-to-moderately *Wfs1* mRNA-hybridized cells were seen in layers II and III. In the rostro-lateral part of the MEA, weak *Wfs1* mRNA signals were detected in layer II (Fig. 7A and B).

In the LEA, strong *Wfs1* mRNA signals were observed in the outer zone of layer III. The distribution of these signals was confined to around the rhinal fissure (Fig. 7A and B). In the other part of the LEA, weak-to-moderate signals were seen in layer III deeper down. Different from the other multi-layered cortical areas, a very small number of *Wfs1* mRNA signals was detected in layer II (Fig. 7A and B).

4. Discussion

In the present study, we determined the patterns of change in the strength of *Wfs1* mRNA signals in each of the mouse brain structures from birth to early adulthood (P8W). There were three patterns. In type 1, signals were weak or absent in neonates but strong or moderate in young adults. This pattern was observed in the CA1 field, the PaS, and in the entorhinal cortex (MEA and LEA). In type 2, signals were of a relatively constant strength during development. This pattern was seen in limbic structures (e.g. S (subiculum) and Ce (central amygdaloid nucleus)) and brainstem nuclei (e.g. facial and chochlear nuclei). In type 3, signals peaked in the second week of age. This pattern was observed in the Rt (thalamic reticular nucleus). The present study also demonstrated layer-specific localization of *Wfs1* mRNA signals in the CA1 field, the PaS, and in the entorhinal cortex where strong signals were seen from P14 to early adulthood (P8W).

4.1. Comparison with previous findings

Our findings on *Wfs1* mRNA expression in the brain of young-adult mice were primarily compatible with previous studies in the mouse (Kato et al., 2008; Kawano et al., 2008; Luuk et al., 2008) and the rat (Takeda et al., 2001). In these studies, *Wfs1* expression was described in the cerebral cortex, the basal ganglia, the hypothalamus, the brain stem motor and sensory nuclei, the reticular formation, and in the cerebellar cortex, as well as in the CA1 field and in the amygdala. The present study showed that *Wfs1* mRNA signals were observed in these structures of the young-adult mouse. The findings indicate that *Wfs1* mRNA expression in these structures (present study) is similar to Wfs1 protein expression (Kato et al., 2008; Luuk et al., 2008), and is similar between the mouse (present study) and the rat (Takeda et al., 2001) in early adulthood.

4.2. Patterns of change in Wfs1 mRNA expression

In the following, we discuss each type of the patterns of change in the strength of *Wfs1* mRNA signals systematically.

4.2.1. Type 1 pattern of change

4.2.1.1. Type 1a. Type 1a pattern was observed in the limbic cortex: the CA1 field, PaS, MEA, and LEA. The CA1 field is a part of the hippocampus proper, and the PaS, MEA, and LEA are parts of the parahippocampal cortical areas (Witter and Amaral, 2004). Detailed discussions about these structures are described separately in Section 4.3.

4.2.1.2. Type 1b. Type 1b pattern was observed in the motor, limbic, and olfactory cortices (MoCII, CgII, and Pir), basal nuclei that are parts of the limbic system (LS, and Acb), and in the sensory and motor brainstem nuclei (Me5, 7MN, and Amb). The cingulate cortex is one of the largest components of the limbic system and is characterized by diffuse projections from the anteromedial thalamic nucleus (Palomero-Gallagher and Zilles, 2004). It is involved in motivational aspects of learning tasks (Gabriel et al., 1980) and contributes to motor functions via numerous efferents to subcortical motor systems (Palomero-Gallagher and Zilles, 2004). The Pir (piriform cortex) is a part of the primary olfactory cortex, since the Pir receives direct projections from the MOB (main olfactory bulb) (Shipley et al., 2004). The LS (lateral septal nucleus) is characterized by massive glutamatergic afferents from the hippocampus proper and the subiculum, and by massive bidirectional connections with the rostral brainstem, especially with the hypothalamus and the ventral midbrain. The LS contributes to emotional behaviors (Risold, 2004). The Acb (nucleus accumbens) is a limbic part of the striatum. This nucleus receives extensive inputs from limbic structures, such as the hippocampus and amygdala, as well as from the prefrontal areas subserving limbic and autonomic functions, i.e. orbital, infralimbic, prelimbic, and agranular insular cortices. The Acb reciprocates its dopaminergic input, and in addition, innervates most of the dopaminergic neurons projecting to the associative and motor structures (Joel and Weiner, 2000). The Me5 (mesencephalic trigeminal nucleus) is one of the sensory relay nuclei, and plays a role in proprioception during mastication and the integration of jaw movements (Waite, 2004). The Amb (nucleus ambiguus) is one of the branchial motor nuclei in the brainstem, and innervates the striated muscles of the pharynx, esophagus, and larynx (Loewy and Spyer, 1990; Saper, 2000). It is possible that the Me5 and the Amb contribute to feeding. Further details concerning the 7NM are described separately in Section 4.4.

4.2.1.3. Type 1c. Type 1c pattern was observed in layer II of the sensory cortical areas except for the olfactory area (SoCII, AuCII, and ViCII), and in the SC. There are some striking similarities between the sensory cortical areas and the SC: both structures have layered architecture, the both structures receive few olfactory inputs, and the both structures contribute to process sensory information including visual, somatosensory, and auditory modalities (Sefton et al., 2004).

4.2.2. Type 2 pattern of change

4.2.2.1. Type 2a. Type 2a pattern was observed in the limbic structures (S, Tu, BSTL, IPAC, and Ce), the caudal part of the CPu, and

in the oromotor nuclei relevant to feeding (Mo5, 7NL, and 12N). The S (subiculum) is a part of the hippocampal formation and is the major origin of the fornix (Witter and Amaral, 2004). The Tu (olfactory tuberculum) is referred to as a part of the primary olfactory cortex, since the Tu receives direct projections from the MOB. In addition, the Tu is regarded as a part of the ventral striatum, the limbic part of the striatum (Shipley et al., 2004). The BSTL (lateral bed nucleus of the stria terminalis) and the IPAC (interstitial nucleus of the posterior limb of the anterior commissure) are parts of the central division of the extended amygdala. This means that characteristics of the BSTL and the IPAC are similar to those of the Ce (central amygdaloid nucleus): the BSTL and the IPAC maintain close structural, cytochemical, and hodological relationships with the Ce (de Olmos et al., 2004). The Ce is believed to be an important output region of the amygdala, at least for the expression of innate emotional responses and associated physiological responses. The expression of these responses involves connections from the medial subdivision of the Ce to brainstem areas that control specific behaviors and physiological responses (LeDoux, 2007).

In general, the CPu (dorsal striatum or neostriatum) is subdivided into medial and lateral from the anato-functional aspect of view. The lateral CPu is regarded as motor striatum, and the medial CPu is regarded as associative striatum (Joel and Weiner, 2000). In addition, anatomical differences between the rostral and caudal CPu were also reported in the rodent striatum. The distribution of μ (mu) opiate receptors demonstrated that spatial organization of patch and matrix compartments in the rat striatum was different between rostral and caudal parts: patches were numerous and of large size in the rostral part, while they were rare and of small size in the caudal part (Desban et al., 1993). As for corticostriatal projections to the matrix in the rat striatum, patterns of axonal arborization were different between the rostral and caudal parts: the extended axonal arborizations were primarily confined to the rostral part, conversely, the focal axonal arborizations were observed most obvious in the caudal part (Kincaid and Wilson, 1996). Since there are anatomical differences between the rostral and caudal parts of the rodent CPu, it is possible to accept that the type 2a pattern of change in the mouse CPu was confined to the caudal part. Further details concerning the oromotor nuclei (Mo5, 7NL, and 12N) are described separately in Section 4.4.

4.2.2.2. Type 2b. Interestingly, brain structures potentially relevant to the clinical symptoms of Wolfram syndrome showed the type 2b pattern of change. Detailed discussions concerning the clinical symptoms are described separately in Sections 4.5–4.7. In addition, brain structures, where atrophic changes were observed in Wolfram syndrome patients, also represented the type 2b pattern. For example, the main and accessory olfactory bulbs (MOB and AOB) showed the type 2b pattern in the mouse. In Wolfram syndrome patients, atrophic changes were observed in the olfactory bulb and tracts (Genís et al., 1997; Shannon et al., 1999). Further details concerning the atrophic changes are given in Section 4.8.

4.2.3. Type 3 pattern of change

4.2.3.1. Type 3a. The Rt (thalamic reticular nucleus), which showed the type 3a pattern, forms a thin neuronal sheet at the rostral, dorsolateral, lateral, and ventrolateral edges of the dorsal thalamus (Groenewegen and Witter, 2004). Groenewegen and Witter (2004) noted that the Rt was strategically "placed" between the dorsal thalamus and the cerebral hemisphere: all incoming and outgoing fibers of the thalamus have to pass through the Rt, and most of the giving off collaterals terminates at a restricted part of the Rt. Thalamic reticular neurons are all GABAergic and express parvalbumin (Mitrofanis, 1992). The prevailing interpretation of the functional role of the Rt is that it serves attentional brain mechanisms (e.g., "searchlight hypothesis") (Crick, 1984; Guillery et al., 1998; McAlonan et al., 2000). The Rt is important for the control of the firing mode of thalamocortical projection neurons and, in this way, for the selection of the information that is transferred from the thalamus to the cerebral cortex. The Rt plays an important role as pacemaker during synchronized firing of thalamocortical cells (Groenewegen and Witter, 2004).

4.2.3.2. Type 3b. Type 3b pattern was observed in layer V of the motor (MoCV), sensory (SoCV, AuCV, and ViCV), and of the limbic cortices (CgV, and RSCV) and in layer II of the limbic cortex (RSCII). Interestingly, *Wfs1* mRNA signals in layer II were observed in the motor, sensory, and cingulate cortices in early adulthood, while those were not seen in the retrosplenial cortex. Together with the anterior cingulate cortex, the retrosplenial cortex is involved in the motivational aspects of learning tasks and contributes to motor functions via numerous efferents to subcortical motor systems (Palomero-Gallagher and Zilles, 2004). In addition, many observations support a significant role of the retrosplenial cortex in visuospatial functions. There is massive visual input to the retrosplenial cortex, and major projections from the postsubiculum which is involved in coding for head position in space (Taube et al., 1990; Vogt et al., 2004).

Interestingly, *Wfs1* mRNA expression in layer V of the motor and sensory cortices (type 3b) synchronized with that in the Rt (type 3a). It is not known why the expression in these structures synchronized each other. It should be noted that layer V in the motor and sensory cortices indirectly connect with the Rt by way of the higher order thalamic nuclei (Gabreëls et al., 1998). For example, layer V neurons in the visual cortex send their axons to the lateral posterior nucleus (LP), a higher order nucleus of the visual thalamus (Sefton et al., 2004). Then LP neurons project to the Rt (Groenewegen and Witter, 2004). The indirect connections between layer V and the Rt may provide clues as to the synchronization.

4.3. Strong Wfs1 mRNA signals in the CA1 field, PaS, and entorhinal cortex

4.3.1. CA1 field

The CA1 field is a part of the hippocampus proper. According to an excellent review by Witter and Amaral (2004), the CA1 field has connections with various intrahippocampal, cortical, and subcortical structures. The CA1 field receives intrahippocampal projections from the CA3 field (Schaffer collaterals), and from the CA2 field (Ishizuka et al., 1990). There are only weak associational connections (Tamamaki et al., 1987; Amaral et al., 1991) and weak commissural connections (Van Groen and Wyss, 1990b) in the CA1 field. Cortical inputs to the CA1 field arise from the entorhinal, perirhinal, and postrhinal cortices, which compose the parahippocampal region. The CA1 field receives subcortical projections from the septum, the amygdala, and from the thalamus. It also receives light noradrenergic, serotonergic, and dopaminergic inputs from the brainstem nuclei (Swanson et al., 1987). In addition to the afferent connections, the CA1 field has efferent connections with various intrahippocampal, cortical, and subcortical structures. The major projection arising from the CA1 field is a projection to the adjacent subiculum. With regard to cortical efferents, the CA1 field sends axons back to the parahippocampal region including the entorhinal, perirhinal, and postrhinal cortices. The CA1 field also projects to the retrosplenial, prelimbic, and infralimbic cortices. Subcortical outputs from the CA1 field terminate in the septum, nucleus

accumbens, olfactory structures including the olfactory bulb, the hypothalamus, and in the amygdala (Van Groen and Wyss, 1990b; Witter and Amaral, 2004). Since strong *Wfs1* mRNA signals were observed in the pyramidal layer, the *Wfs1* gene might contribute to these neuronal relays in this layer. However, it is unclear whether *Wfs1* mRNA-hybridized pyramidal cells are involved in all of these neuronal relays. Further studies by using tract-tracing methods are required to clarify the fiber connections of *Wfs1* mRNA-hybridized neurons in the CA1 field.

The principal neuronal cell type of the CA1 field is the pyramidal cell (Witter and Amaral, 2004). Since the pyramidal cell makes up the vast majority of neurons in the pyramidal cell layer (Witter and Amaral, 2004), and since *Wfs1* mRNA signals were seen in most of the cells of this layer (present study), the signals were probably located in pyramidal cells. In addition to the pyramidal cell, there are several types of non-pyramidal cells in strata oriens, radiatum, and lacunosum-moleculare of the CA1 field. The vast majority of these neurons are immunoreactive for GABA (γ-aminobutyric acid; Ribak et al., 1978), and most of these cells are considered to be local circuit neurons (interneurons; Witter and Amaral, 2004). Since *Wfs1* mRNA-hybridized cells were also observed in strata radiatum and oriens of the CA1 field (present study), it is suggested that *Wfs1* mRNA would be detected in interneurons of these strata. However, it is not known whether *Wfs1* mRNA signals are present in interneurons of the pyramidal cell layer. Further studies are required to clarify whether *Wfs1* mRNA is expressed in interneurons of the pyramidal cell layer in the CA1 field.

Functional studies suggested that the septal hippocampus is necessary for spatial learning and memory (Moser et al., 1993; Witter and Amaral, 2004), whereas the temporal hippocampus appears to be essential for normal fear-related behavior in rats (Kjelstrup et al., 2002; Witter and Amaral, 2004). Since *Wfs1* mRNA signals in the CA1 field were observed in both the septal and temporal levels, the *Wfs1* gene might contribute both to spatial learning and memory, and to normal fear-related behavior. In addition, distribution of the signals was not homogeneous in the CA1 field: strong signals were observed in the septal hippocampus while weak-to-moderate signals were seen in the temporal hippocampus (present study). The functional difference between the septal and temporal hippocampi may help to explain the difference in the strength of the signals between the two hippocampi.

4.3.2. PaS

The PaS is one of the parahippocampal areas. In the mouse, *Wfs1* mRNA signals were confined to layers II and III (the external lamina). Afferent fibers to these layers arise from various intrinsic, hippocampal, parahippocampal, cortical, and subcortical structures in the rat (Witter and Amaral, 2004). The PaS gives rise to both intrinsic associational connections (Köhler, 1985; Caballero-Bleda and Witter, 1993), and a commissural projection (Köhler, 1985; Van Groen and Wyss, 1990a). The PaS receives a hippocampal input from the subiculum (Swanson et al., 1978; Köhler, 1985; Van Groen and Wyss, 1990a,c), and a weak parahippocampal input from the entorhinal cortex (Köhler, 1986, 1988; Van Groen and Wyss, 1990a,c). The PaS also receives weak cortical projections from the retrosplenial cortex and the occipital visual cortex (Vogt and Miller, 1983; Van Groen and Wyss, 1990a). Subcortical afferents to the PaS arise from the septum, the endopiriform nucleus (Van Groen and Wyss, 1990a,c; Eid et al., 1996; Behan and Haberly, 1999), amygdala (Van Groen and Wyss, 1990a; Petrovich et al., 1996; Pikkarainen et al., 1999; Kemppainen et al., 2002), and the thalamus. Thalamic inputs to the PaS arise from the anteroventral and anterodorsal nuclei, laterodorsal nucleus, and nucleus reuniens (Herkenham, 1978; Wouterlood et al., 1990; Shibata, 1993; Van Groen and Wyss, 1995). The PaS receives serotonergic projections from the raphe nuclei (Köhler et al., 1981; Köhler and Steinbusch, 1982; Van Groen and Wyss, 1990a,c), and noradrenergic projection from the locus coeruleus (Swanson et al., 1987; Witter and Amaral, 2004).

In addition to receiving afferent fibers, the PaS sends efferent fibers to hippocampal, parahippocampal, and subcortical structures (Witter and Amaral, 2004). The PaS gives rise to hippocampal projections to the dentate gyrus, the hippocampus proper, and to the subiculum (Köhler, 1985; Van Groen and Wyss, 1990a). It sends parahippocampal projections to the presubiculum (Köhler, 1985; Van Groen and Wyss, 1990a) and to the entorhinal cortex (Köhler, 1985; Van Groen and Wyss, 1990a; Caballero-Bleda and Witter, 1993), and gives rise to a modest thalamic projection to the anterodorsal nucleus. This nucleus is the exclusive target of the extrahippocampal projections in the rat PaS (Van Groen and Wyss, 1990a; Witter and Amaral, 2004). As described above, the PaS is involved in several neuronal relays. Probably the most unique characteristic of the PaS is its relay from the anterior thalamic nucleus to the hippocampal formation. This relay provides a route by which thalamic input might influence very early stages of hippocampal information processing (Witter and Amaral, 2004). The *Wfs1* gene possibly contributes to this information processing.

4.3.3. Entorhinal cortex

4.3.3.1. Fiber connections of the superficial layers of the entorhinal cortex. The entorhinal cortex (MEA and LEA) is a part of the parahippocampal cortex. According to the review by Witter and Amaral (2004), fibers of the so-called perforant pathway take their origin mainly from entorhinal-cortical neurons located in layers II and III, where *Wfs1* mRNA signals were observed in the mouse. These layers receive inputs from a variety of cortical structures including the ipsilateral and contralateral entorhinal cortex (Burwell and Amaral, 1998b). Extrinsic cortical afferents to the superficial layers originate from the hippocampal and parahippocampal regions. Hippocampal fibers to the layers arise from the subiculum, and parahippocampal afferents originate from the perirhinal and postrhinal cortices, the presubiculum (Naber et al., 1997; Burwell and Amaral, 1998a,b), and from the PaS (Köhler, 1985; Van Groen and Wyss, 1990a; Caballero-Bleda and Witter, 1993). Finally, a substantial input to the superficial layers originates from the olfactory structures, in particular from the olfactory bulb, the anterior olfactory nucleus, and the piriform cortex (Haberly and Price, 1978; Kosel et al., 1981). In addition, the superficial layers receive subcortical afferents from the telencephalon, the thalamus, the hypothalamus, and the brainstem. Telencephalic inputs arise from the medial septal nucleus, nucleus of the diagonal band, and from the amygdala (Price et al., 1987; Pitkänen et al., 2000). The major thalamic input originates from nucleus reunions (Herkenham, 1978; Wouterlood et al., 1990; Wouterlood, 1991). The hypothalamic input arises from the supramammillary nucleus (Haglund et al., 1984). The brainstem input originates from the ventral tegmental area, the central and dorsal raphe nuclei (Azmitia and Segal, 1978; Köhler and Steinbusch, 1982), locus coeruleus (Moore et al., 1978), and from nucleus incertus, a CRH (corticotropin releasing hormone) receptor-rich nucleus (Goto et al., 2001; Witter and Amaral, 2004).

In addition to these afferent connections, the superficial layers have efferent connections not only with the hippocampal formation (the perforant pathway), but also with parahippocampal, limbic, paralimbic, and olfactory regions of the cortex (Insausti et al., 1997) and with the septal region (Alonso and Köhler, 1984). Perforant path fibers terminate in the dentate gyrus, the CA3 and CA1 fields, and in the subiculum (Witter and Amaral, 2004), and the perforant pathway is most likely glutamatergic (Fonnum,

1970). Parahippocampal projections from the superficial layers terminate in the presubiculum, the PaS (Köhler, 1986, 1988; Van Groen and Wyss, 1990a,c), and in perirhinal area 35 (Insausti et al., 1997; Burwell and Amaral, 1998a). The superficial layers emit projections to the infralimbic cortex, the ventral taenia tecta, the prelimbic, orbitofrontal, and agranular insular cortices (Wyss and Van Groen, 1992; Condé et al., 1995; Insausti et al., 1997), and the olfactory area (de Olmos et al., 1978; Insausti et al., 1997). Additionally, many layer II neurons in the MEA project to the septal region (Alonso and Köhler, 1984; Witter and Amaral, 2004). Thus, it is possible that *Wfs1* mRNA-hybridized cells in layers II and III of the entorhinal cortex are involved in a wide variety of neuronal relays through the perforant pathway described above. Since neurons in these layers are key elements in the temporal lobe memory system (Klink and Alonso, 1997), the *Wfs1* mRNA-hybridized cells contribute to learning and memory. However, it is unclear whether majority of perforant pathway neurons in these layers express *Wfs1* mRNA. Further studies by using tract-tracing methods are required to clarify the fiber connections of *Wfs1* mRNA-hybridized neurons in the entorhinal cortex. Such studies will uncover whether the *Wfs1* mRNA-hybridized cells contribute to learning and memory as projection neurons (perforant pathway neurons) or interneurons.

4.3.3.2. The islet of cells in layer II of the MEA. The present study demonstrated the islet of cells in layer II of the mouse MEA. A majority of the cells in the islet were strongly hybridized with *Wfs1* mRNA. This evidence is supported by the finding that highly Wfs1-positive cell clusters were distributed in the mouse MEA (Luuk et al., 2008; Kawano et al., unpublished observations). Although Woznicka et al. (2006) demonstrated that "distinct spherical groups of small cells are situated at the border of layer I/II" in the caudal part of the canine MEA, there have been few descriptions of the islet in both the mouse and the rat (Insausti et al., 1997; van Groen, 2001; Witter and Amaral, 2004). Further studies are required to clarify hodological, neurophysiological, histochemical, and immunohistochemical details of the islet. In such studies, *Wfs1* mRNA will be a useful marker for the islet.

4.3.3.3. A small number of Wfs1 mRNA signals in layer II of the LEA. A laminar distribution of *Wfs1* mRNA and protein in layer II was present in most of the mouse cortical areas (Kawano et al., 2008; Luuk et al., 2008; Kawano et al., unpublished observation) as described in the rat (Takeda et al., 2001). In the LEA, *Wfs1* mRNA signals were observed in layer III, however, only a small number of the signals was detected in layer II. This evidence suggests that the laminar distribution of *Wfs1* mRNA signals in the LEA is unique to that in the multi-layered cortex. Thus *Wfs1* mRNA might be a useful marker to distinguish the LEA from other cortical areas including the MEA.

4.4. Facial nucleus

In the facial nucleus, the pattern of change in the strength of *Wfs1* mRNA signals differed between the 7NM (type 1b) and the 7NL (type 2a). This difference might be attributable to the myotopical organization in the nucleus. The facial nucleus in rodents is myotopically organized from birth to adulthood: neurons in the 7NM innervate the auricular muscles, whereas those in the 7NL send their axons to muscles in the orbital region, the perioral region, and in the proboscis (muscles involved with orofacial function) (Ashwell, 1982; Ashwell and Watson, 1983; Travers, 2004). It is not known why the type 1b pattern is seen in the 7NM, however, it is possible that the type 2a pattern in the 7NL is attributable to the orofacial function especially feeding, since the same pattern of change (type 2a) was seen in the Mo5 (motor nucleus of the trigeminal nerve) and in the 12N (hypoglossal nucleus), which play important roles in feeding.

4.5. Diabetes insipidus

Arginine vasopressin-synthesizing neurons are distributed in the SO (supraoptic nucleus) and the PVNm (magnocellular part of the paraventricular hypothalamic nucleus) (Armstrong, 2004). *Wfs1* mRNA signals in these nuclei showed the type 2b pattern (Figs. 1, 3G–L; Table 1). This finding suggests that the diabetes insipidus in Wolfram syndrome patients is attributable to dysfunctional neurons in these nuclei resulting from loss-of-function mutations in the *WFS1* gene.

Neuropathological studies showed loss of neurons in the SO and in the paraventricular hypothalamic nucleus (Genís et al., 1997; Shannon et al., 1999). In addition, Gabreëls et al. (1998) examined brains of three Wolfram syndrome patients by using immunohistochemistry for both the vasopressin and for the vasopressin precursor, and described in the patients with diabetes insipidus, not only a loss of the vasopressin in neurons of the paraventricular hypothalamic nucleus, but also a defect in processing of the vasopressin precursor in this nucleus. Thus, the WFS1 protein may function in the survival of neurons and in vasopressin precursor-processing from birth to early adulthood in the SO and/or the PVNm.

4.6. Sensorineural hearing loss

The *WFS1* gene is responsible for both sensorineural deafness in Wolfram syndrome patients (Minton et al., 2003) and autosomal dominant low frequency sensorineural hearing loss (Bespalova et al., 2001; Young et al., 2001). In the mouse brain, *Wfs1* mRNA signals in the cochlear nucleus and inferior colliculus showed the type 2b pattern, and those in the auditory cortex, the type 1c or 3b pattern. In the cochlea, Wfs1 protein was invariably expressed in inner hair cells and spiral ganglion cells from birth to postnatal day 35 (Cryns et al., 2003). Thus, it is suggested that the *Wfs1* gene contributes to both the development and maintenance of cells in the auditory system including the cochlea. It is also suggested that not only dysfunctional inner ear cells but also dysfunctional neurons in the auditory-related structures of the brain attribute to both the sensorineural deafness in Wolfram syndrome patients and autosomal dominant low frequency sensorineural hearing loss.

4.7. Psychiatric symptoms in Wolfram syndrome patients

Swift et al. (1990) reported that 41 of 68 Wolfram syndrome patients (60%) had episodes of severe depression, psychosis, or organic brain syndrome, as well as impulsive verbal and physical aggression. These symptoms were very severe in 17 patients (25%), of whom 12 required admission to a psychiatric hospital and 11 attempted suicide. Based on this evidence, they proposed that the *WFS1* gene predisposed homozygotes to psychiatric illness (Swift et al., 1990). Subsequently, molecular neuropsychiatric studies suggested a role for the *WFS1* gene in the pathophysiology of impulsive suicide (Sequeira et al., 2003), and an association between mutations of the *WFS1* gene and hospitalization for psychiatric illness (Swift and Swift, 2005). In addition, the *Wfs1* gene was suggested to be a putative biomarker for post-traumatic stress disorder by a behavioral study using rats (Kesner et al., 2007), and the *Wfs1* knockout mouse showed bipolar disorder-like behavioral phenotypes, such as retardation in emotionally triggered behavior, decreased social interaction, and altered behavioral despair depending on experimental conditions (Kato

et al., 2008). Conversely, several molecular neuropsychiatric studies have found no evidence of a supporting role for the *WFS1* gene in psychiatric disorders, particularly major depression and bipolar disorder (Furlong et al., 1999; Evans et al., 2000; Middle et al., 2000; Ohtsuki et al., 2000; Kato et al., 2003; Kawamoto et al., 2004). As described here, it is not known whether mutations of the *WFS1* gene contribute significantly to the incidence of psychiatric illness. The present study showed that weak *Wfs1* mRNA signals were distributed in the raphe nuclei and nucleus coeruleus from birth to early adulthood. It is possible that the functions of the raphe nuclei and of the nucleus coeruleus in Wolfram syndrome patients are impaired by loss-of-function mutations in the *WFS1* gene. The dysfunction may predispose the patients to major depression and bipolar disorder, since these nuclei are strongly related to these mood disorders (Kandel, 2000). In addition, the present study demonstrated that strong-to-moderate *Wfs1* mRNA signals were widely distributed in the limbic structures including the hippocampus and the amygdala, and in the rostral part of the cerebral cortex from P14 to early adulthood. It is possible that the psychiatric symptoms in Wolfram syndrome patients are attributable to dysfunctional neurons in these structures arising from loss-of-function mutations in the *WFS1* gene.

4.8. Relationship between Wfs1 mRNA expression and neuroradiological and neuropathological evidence

Neuroradiological (Rando et al., 1992; Scolding et al., 1996; Ito et al., 2007) and neuropathological (Genís et al., 1997; Shannon et al., 1999) examinations have been carried out in brains of Wolfram patients. The principal findings of these examinations were brainstem atrophy, cerebellar atrophy, and optic atrophy. Mild atrophic changes in the cerebral cortex and hypothalamus were also described. The present study showed that strong-to-moderate *Wfs1* mRNA signals were widely seen in the limbic structures (e.g. CA1, MEA, LEA, PaS, S, Tu, BSTL, IPAC, and Ce) from P7 to early adulthood. However, these structures were not affected in Wolfram syndrome patients (Genís et al., 1997; Shannon et al., 1999). Although *Wfs1* mRNA signals in the cerebellar cortex were weak from P4 to early adulthood (type 2b), cerebellar atrophy was demonstrated in Wolfram syndrome patients (Rando et al., 1992; Scolding et al., 1996; Genís et al., 1997; Shannon et al., 1999; Ito et al., 2007).

To reconcile the results with the neuroradiological and neuropathological evidence, the following possible interpretations are offered. In the cerebellum, functions of the WFS1 protein are essential for the survival of neurons expressing weak *WFS1* mRNA signals. In the limbic structures, functions of the WFS1 protein are not necessary for the survival of neurons expressing strong-to-moderate *WFS1* mRNA signals and/or functions of the mutant WFS1 protein are counteracted in these neurons by 'functionally-related proteins of WFS1 (WFS1-frps)', which compensate for functions of the normal WFS1 protein. Thus pathological changes do not occur in the limbic structures, but do occur in the cerebellum.

Interestingly, several nuclei potentially relevant to the symptoms of Wolfram syndrome, such as the SO and PVNm, potentially relevant to diabetes insipidus; the Co and IC, potentially relevant to sensorineural hearing loss; and the LC and raphe nuclei, potentially relevant to psychiatric symptoms, also showed the type 2b pattern the same as the cerebellum. These results support the notion that functions of the WFS1 protein are essential for the survival of neurons expressing weak *WFS1* mRNA signals in symptom-relevant nuclei, the WFS1-frps are not expressed in the neurons, and these factors lead to pathological changes in the symptom-relevant nuclei of Wolfram syndrome patients.

4.9. Conclusion

There were three patterns of change in the strength of *Wfs1* mRNA signals in each of the mouse brain structures during the postnatal development. Out of the three patterns, several nuclei potentially relevant to the symptoms of Wolfram syndrome showed the type 2b pattern, in which the signals were weak and of a relatively constant strength during development. Based on these results, the present study provided a hypothesis that functions of the WFS1 protein are essential for the survival of neurons expressing weak *WFS1* mRNA signals in symptom-relevant nuclei, the WFS1-frps are not expressed in the neurons, and these factors lead to pathological changes in the symptom-relevant nuclei of Wolfram syndrome patients. To test this hypothesis experimentally, the availability of the *Wfs1* knockout mouse could offer opportunities for further investigation. These studies in the next step are necessary to determine the exact physiological role of the Wfs1 protein in the brain, and to obtain more insights into its pathophysiological roles in the endocrinological, otological, neurological, and psychiatric symptoms of Wolfram syndrome.

Acknowledgements

The first and corresponding author, June Kawano, thanks Professor Shiro Nakagawa (Laboratory for Neuroanatomy, Department of Neurology, Kagoshima University Graduate School of Medical and Dental Sciences) for encouragement and for valuable discussions. This study was supported in part by a Grant-in-aid for Scientific Research (C) (15591228 to J.K.) from The Japan Society for the Promotion of Science (JSPS), a Grant-in-aid for Scientific Research on Priority Areas (19040020 to K.S.) from The Ministry of Education, Culture, Sports, Science and Technology (MEXT), and in part by Kodama Memorial Fund Medical Research (2006-100 to J.K.).

References

Alonso, A., Köhler, C., 1984. A study of the reciprocal connections between the septum and the entorhinal area using anterograde and retrograde axonal transport methods in the rat brain. J. Comp. Neurol. 225, 327–343.
Amaral, D.G., Dolorfo, C., Alvarez-Royo, P., 1991. Organization of CA1 projections to the subiculum: a PHA-L analysis in the rat. Hippocampus 1, 415–435.
Armstrong, W.E., 2004. Hypothalamic supraoptic and paraventricular nuclei. In: Paxinos, G. (Ed.), The Rat Nervous System. third ed. Elsevier Academic Press, San Diego, pp. 369–388.
Ashwell, K.W., 1982. The adult mouse facial nerve nucleus: morphology and musculotopic organization. J. Anat. 135, 531–538.
Ashwell, K.W., Watson, C.R., 1983. The development of facial motoneurones in the mouse—neuronal death and the innervation of the facial muscles. J. Embryol. Exp. Morphol. 77, 117–141.
Azmitia, E.C., Segal, M., 1978. An autoradiographic analysis of the differential ascending projections of the dorsal and median raphe nuclei in the rat. J. Comp. Neurol. 179, 641–667.
Barrett, T.G., Bundey, S.E., Macleod, A.F., 1995. Neurodegeneration and diabetes: UK nationwide study of Wolfram (DIDMOAD) syndrome. Lancet 346, 1458–1463.
Behan, M., Haberly, L.B., 1999. Intrinsic and efferent connections of the endopiriform nucleus in rat. J. Comp. Neurol. 408, 532–548.
Bespalova, I.N., Van Camp, G., Bom, S.J., Brown, D.J., Cryns, K., DeWan, A.T., Erson, A.E., Flothmann, K., Kunst, H.P., Kurnool, P., Sivakumaran, T.A., Cremers, C.W., Leal, S.M., Burmeister, M., Lesperance, M.M., 2001. Mutations in the Wolfram syndrome 1 gene (*WFS1*) are a common cause of low frequency sensorineural hearing loss. Hum. Mol. Genet. 10, 2501–2508.
Burwell, R.D., Amaral, D.G., 1998a. Perirhinal and postrhinal cortices of the rat: interconnectivity and connections with the entorhinal cortex. J. Comp. Neurol. 391, 293–321.
Burwell, R.D., Amaral, D.G., 1998b. Cortical afferents of the perirhinal, postrhinal, and entorhinal cortices of the rat. J. Comp. Neurol. 398, 179–205.
Caballero-Bleda, M., Witter, M.P., 1993. Regional and laminar organization of projections from the presubiculum and parasubiculum to the entorhinal cortex: an anterograde tracing study in the rat. J. Comp. Neurol. 328, 115–129.
Cano, A., Rouzier, C., Monnot, S., Chabrol, B., Conrath, J., Lecomte, P., Delobel, B., Boileau, P., Valero, R., Procaccio, V., Paquis-Flucklinger, V., Vialettes, B., 2007. Identification of novel mutations in *WFS1* and genotype–phenotype correlation in Wolfram syndrome. Am. J. Med. Genet. A 143A, 1605–1612.

Collier, D.A., Barrett, T.G., Curtis, D., Macleod, A., Arranz, M.J., Maassen, J.A., Bundey, S., 1996. Linkage of Wolfram syndrome to chromosome 4p16.1 and evidence for heterogeneity. Am. J. Hum. Genet. 59, 855–863.
Condé, F., Maire-Lepoivre, E., Audinat, E., Crépel, F., 1995. Afferent connections of the medial frontal cortex of the rat. II. Cortical and subcortical afferents. J. Comp. Neurol. 352, 567–593.
Crick, F., 1984. Function of the thalamic reticular complex: the searchlight hypothesis. Proc. Natl. Acad. Sci. U.S.A. 81, 4586–4590.
Cryns, K., Thys, S., Van Laer, L., Oka, Y., Pfister, M., Van Nassauw, L., Smith, R.J., Timmermans, J.P., Van Camp, G., 2003. The *WFS1* gene, responsible for low frequency sensorineural hearing loss and Wolfram syndrome, is expressed in a variety of inner ear cells. Histochem. Cell Biol. 119, 247–256.
de Olmos, J., Hardy, H., Heimer, L., 1978. The afferent connections of the main and the accessory olfactory bulb formations in the rat: an experimental HRP-study. J. Comp. Neurol. 181, 213–244.
de Olmos, J.S., Beltramino, C.A., Alheid, G., 2004. Amygdala and extended amygdala of the rat: a cytoarchitectonical, fibroarchitectonical, and chemoarchitectonical survey. In: Paxinos, G. (Ed.), The Rat Nervous System. third ed. Elsevier Academic Press, San Diego, pp. 509–603.
Desban, M., Kemel, M.L., Glowinski, J., Gauchy, C., 1993. Spatial organization of patch and matrix compartments in the rat striatum. Neuroscience 57, 661–671.
Eid, T., Jorritsma-Byham, B., Schwarcz, R., Witter, M.P., 1996. Afferents to the seizure-sensitive neurons in layer III of the medial entorhinal area: a tracing study in the rat. Exp. Brain Res. 109, 209–218.
Evans, K.L., Lawson, D., Meitinger, T., Blackwood, D.H., Porteous, D.J., 2000. Mutational analysis of the Wolfram syndrome gene in two families with chromosome 4p-linked bipolar affective disorder. Am. J. Med. Genet. 96, 158–160.
Fonnum, F., 1970. Topographical and subcellular localization of choline acetyltransferase in rat hippocampal region. J. Neurochem. 17, 1029–1037.
Fonseca, S.G., Fukuma, M., Lipson, K.L., Nguyen, L.X., Allen, J.R., Oka, Y., Urano, F., 2005. WFS1 is a novel component of the unfolded protein response and maintains homeostasis of the endoplasmic reticulum in pancreatic β-cells. J. Biol. Chem. 280, 39609–39615.
Furlong, R.A., Ho, L.W., Rubinsztein, J.S., Michael, A., Walsh, C., Paykel, E.S., Rubinsztein, D.C., 1999. A rare coding variant within the *wolframin* gene in bipolar and unipolar affective disorder cases. Neurosci. Lett. 277, 123–126.
Gabreëls, B.A., Swaab, D.F., de Kleijn, D.P., Dean, A., Seidah, N.G., Van de Loo, J.W., Van de Ven, W.J., Martens, G.J., Van Leeuwen, F.W., 1998. The vasopressin precursor is not processed in the hypothalamus of Wolfram syndrome patients with diabetes insipidus: evidence for the involvement of PC2 and 7B2. J. Clin. Endocrinol. Metab. 83, 4026–4033.
Gabriel, M., Foster, K., Orona, E., 1980. Interaction of laminae of the cingulate cortex with the anteroventral thalamus during behavioral learning. Science 208, 1050–1052.
Genís, D., Dávalos, A., Molins, A., Ferrer, I., 1997. Wolfram syndrome: a neuropathological study. Acta Neuropathol. (Berl.) 93, 426–429.
Goto, M., Swanson, L.W., Canteras, N.S., 2001. Connections of the nucleus incertus. J. Comp. Neurol. 438, 86–122.
Groenewegen, H.J., Witter, M.P., 2004. Thalamus. In: Paxinos, G. (Ed.), The Rat Nervous System. third ed. Elsevier Academic Press, San Diego, pp. 407–453.
Guillery, R.W., Feig, S.L., Lozsádi, D.A., 1998. Paying attention to the thalamic reticular nucleus. Trends Neurosci. 21, 28–32.
Gómez-Zaera, M., Strom, T.M., Rodríguez, B., Estivill, X., Meitinger, T., Nunes, V., 2001. Presence of a major WFS1 mutation in Spanish Wolfram syndrome pedigrees. Mol. Genet. Metab. 72, 72–81.
Haberly, L.B., Price, J.L., 1978. Association and commissural fiber systems of the olfactory cortex of the rat. J. Comp. Neurol. 178, 711–740.
Haglund, L., Swanson, L.W., Köhler, C., 1984. The projection of the supramammillary nucleus to the hippocampal formation: an immunohistochemical and anterograde transport study with the lectin PHA-L in the rat. J. Comp. Neurol. 229, 171–185.
Hardy, C., Khanim, F., Torres, R., Scott-Brown, M., Seller, A., Poulton, J., Collier, D., Kirk, J., Polymeropoulos, M., Latif, F., Barrett, T., 1999. Clinical and molecular genetic analysis of 19 Wolfram syndrome kindreds demonstrating a wide spectrum of mutations in WFS1. Am. J. Hum. Genet. 65, 1279–1290.
Herkenham, M., 1978. The connections of the nucleus reuniens thalami: evidence for a direct thalamo-hippocampal pathway in the rat. J. Comp. Neurol. 177, 589–610.
Hofmann, S., Philbrook, C., Gerbitz, K.D., Bauer, M.F., 2003. Wolfram syndrome: structural and functional analyses of mutant and wild-type wolframin, the WFS1 gene product. Hum. Mol. Genet. 12, 2003–2012.
Inoue, H., Tanizawa, Y., Wasson, J., Behn, P., Kalidas, K., Bernal-Mizrachi, E., Mueckler, M., Marshall, H., Donis-Keller, H., Crock, P., Rogers, D., Mikuni, M., Kumashiro, H., Higashi, K., Sobue, G., Oka, Y., Permutt, M.A., 1998. A gene encoding a transmembrane protein is mutated in patients with diabetes mellitus and optic atrophy (Wolfram syndrome). Nat. Genet. 20, 143–148.
Insausti, R., Herrero, M.T., Witter, M.P., 1997. Entorhinal cortex of the rat: cytoarchitectonic subdivisions and the origin and distribution of cortical efferents. Hippocampus 7, 146–183.
Ishihara, H., Takeda, S., Tamura, A., Takahashi, R., Yamaguchi, S., Takei, D., Yamada, T., Inoue, H., Soga, H., Katagiri, H., Tanizawa, Y., Oka, Y., 2004. Disruption of the *WFS1* gene in mice causes progressive β-cell loss and impaired stimulus-secretion coupling in insulin secretion. Hum. Mol. Genet. 13, 1159–1170.
Ishizuka, N., Weber, J., Amaral, D.G., 1990. Organization of intrahippocampal projections originating from CA3 pyramidal cells in the rat. J. Comp. Neurol. 295, 580–623.
Ito, S., Sakakibara, R., Hattori, T., 2007. Wolfram syndrome presenting marked brain MR imaging abnormalities with few neurologic abnormalities. AJNR Am. J. Neuroradiol. 28, 305–306.
Joel, D., Weiner, I., 2000. The connections of the dopaminergic system with the striatum in rats and primates: an analysis with respect to the functional and compartmental organization of the striatum. Neuroscience 96, 451–474.
Kandel, E.R., 2000. Disorders of mood: depression, mania, and anxiety disorders. In: Kandel, E.R., Schwartz, J.H., Jessell, T.M. (Eds.), Principles of Neural Science. fourth ed. McGraw-Hill, New York, pp. 1209–1226.
Kato, T., Ishiwata, M., Yamada, K., Kasahara, T., Kakiuchi, C., Iwamoto, K., Kawamura, K., Ishihara, H., Oka, Y., 2008. Behavioral and gene expression analyses of Wfs1 knockout mice as a possible animal model of mood disorder. Neurosci. Res. 61, 143–158.
Kato, T., Iwamoto, K., Washizuka, S., Mori, K., Tajima, O., Akiyama, T., Nanko, S., Kunugi, H., Kato, N., 2003. No association of mutations and mRNA expression of WFS1/wolframin with bipolar disorder in humans. Neurosci. Lett. 338, 21–24.
Kawamoto, T., Horikawa, Y., Tanaka, T., Kabe, N., Takeda, J., Mikuni, M., 2004. Genetic variations in the WFS1 gene in Japanese with type 2 diabetes and bipolar disorder. Mol. Genet. Metab. 82, 238–245.
Kawano, J., Tanizawa, Y., Shinoda, K., 2008. Wolfram syndrome 1 (*Wfs1*) gene expression in the normal mouse visual system. J. Comp. Neurol. 510, 1–23.
Kemppainen, S., Jolkkonen, E., Pitkänen, A., 2002. Projections from the posterior cortical nucleus of the amygdala to the hippocampal formation and parahippocampal region in rat. Hippocampus 12, 735–755.
Kesner, Y., Zohar, J., Merenlender, A., Gispan, I., Shalit, F., Yadid, G., 2007. *WFS1* gene as a putative biomarker for development of post-traumatic syndrome in an animal model. Mol. Psychiatry. Advance online publication on October 30, 2007. doi:10.1038/sj.mp.4002109.
Khanim, F., Kirk, J., Latif, F., Barrett, T.G., 2001. WFS1/wolframin mutations, Wolfram syndrome, and associated diseases. Hum. Mutat. 17, 357–367.
Kincaid, A.E., Wilson, C.J., 1996. Corticostriatal innervation of the patch and matrix in the rat neostriatum. J. Comp. Neurol. 374, 578–592.
Kjelstrup, K.G., Tuvnes, F.A., Steffenach, H.A., Murison, R., Moser, E.I., Moser, M.B., 2002. Reduced fear expression after lesions of the ventral hippocampus. Proc. Natl. Acad. Sci. U.S.A. 99, 10825–10830.
Klink, R., Alonso, A., 1997. Muscarinic modulation of the oscillatory and repetitive firing properties of entorhinal cortex layer II neurons. J. Neurophysiol. 77, 1813–1828.
Kosel, K.C., Van Hoesen, G.W., West, J.R., 1981. Olfactory bulb projections to the parahippocampal area of the rat. J. Comp. Neurol. 198, 467–482.
Köhler, C., 1985. Intrinsic projections of the retrohippocampal region in the rat brain. I. The subicular complex. J. Comp. Neurol. 236, 504–522.
Köhler, C., 1986. Intrinsic connections of the retrohippocampal region in the rat brain. II. The medial entorhinal area. J. Comp. Neurol. 246, 149–169.
Köhler, C., 1988. Intrinsic connections of the retrohippocampal region in the rat brain. III. The lateral entorhinal area. J. Comp. Neurol. 271, 208–228.
Köhler, C., Chan-Palay, V., Steinbusch, H., 1981. The distribution and orientation of serotonin fibers in the entorhinal and other retrohippocampal areas. An immunohistochemical study with anti-serotonin antibodies in the rats brain. Anat. Embryol. (Berl.) 161, 237–264.
Köhler, C., Steinbusch, H., 1982. Identification of serotonin and non-serotonin-containing neurons of the mid-brain raphe projecting to the entorhinal area and the hippocampal formation. A combined immunohistochemical and fluorescent retrograde tracing study in the rat brain. Neuroscience 7, 951–975.
LeDoux, J., 2007. The amygdala. Curr. Biol. 17, R868–R874.
Loewy, A.D., Spyer, K.M. (Eds.), 1990. Central Regulation of Autonomic Function. Oxford University Press, New York.
Luuk, H., Koks, S., Plaas, M., Hannibal, J., Rehfeld, J.F., Vasar, E., 2008. Distribution of Wfs1 protein in the central nervous system of the mouse and its relation to clinical symptoms of the Wolfram syndrome. J. Comp. Neurol. 509, 642–660.
McAlonan, K., Brown, V.J., Bowman, E.M., 2000. Thalamic reticular nucleus activation reflects attentional gating during classical conditioning. J. Neurosci. 20, 8897–8901.
Middle, F., Jones, I., McCandless, F., Barrett, T., Khanim, F., Owen, M.J., Lendon, C., Craddock, N., 2000. Bipolar disorder and variation at a common polymorphism (A1832G) within exon 8 of the Wolfram gene. Am. J. Med. Genet. 96, 154–157.
Minton, J.A., Hattersley, A.T., Owen, K., McCarthy, M.I., Walker, M., Latif, F., Barrett, T., Frayling, T.M., 2002. Association studies of genetic variation in the *WFS1* gene and type 2 diabetes in U.K. populations. Diabetes 51, 1287–1290.
Minton, J.A., Rainbow, L.A., Ricketts, C., Barrett, T.G., 2003. Wolfram syndrome. Rev. Endocr. Metab. Disord. 4, 53–59.
Mitrofanis, J., 1992. Calbindin immunoreactivity in a subset of cat thalamic reticular neurons. J. Neurocytol. 21, 495–505.
Moore, R.Y., Ziegler, B., Bayer, S.A., 1978. Monoamine neuron innervation of the hippocampal formation: alteration by neonatal irradiation. Exp. Neurol. 60, 318–326.
Moser, E., Moser, M.B., Andersen, P., 1993. Spatial learning impairment parallels the magnitude of dorsal hippocampal lesions, but is hardly present following ventral lesions. J. Neurosci. 13, 3916–3925.
Naber, P.A., Caballero-Bleda, M., Jorritsma-Byham, B., Witter, M.P., 1997. Parallel input to the hippocampal memory system through peri- and postrhinal cortices. Neuroreport 8, 2617–2621.
Ohtsuki, T., Ishiguro, H., Yoshikawa, T., Arinami, T., 2000. *WFS1* gene mutation search in depressive patients: detection of five missense polymorphisms but no association with depression or bipolar affective disorder. J. Affect. Disord. 58, 11–17.

Osman, A.A., Saito, M., Makepeace, C., Permutt, M.A., Schlesinger, P., Mueckler, M., 2003. Wolframin expression induces novel ion channel activity in endoplasmic reticulum membranes and increases intracellular calcium. J. Biol. Chem. 278, 52755–52762.

Palomero-Gallagher, N., Zilles, K., 2004. Isocortex. In: Paxinos, G. (Ed.), The Rat Nervous System. third ed. Elsevier Academic Press, San Diego, pp. 729–757.

Paxinos, G., Franklin, K.B.J., 2001. The Mouse Brain in Stereotaxic Coordinates, second ed. Academic Press, San Diego.

Petrovich, G.D., Risold, P.Y., Swanson, L.W., 1996. Organization of projections from the basomedial nucleus of the amygdala: a PHAL study in the rat. J. Comp. Neurol. 374, 387–420.

Pikkarainen, M., Rönkkö, S., Savander, V., Insausti, R., Pitkänen, A., 1999. Projections from the lateral, basal, and accessory basal nuclei of the amygdala to the hippocampal formation in rat. J. Comp. Neurol. 403, 229–260.

Pitkänen, A., Pikkarainen, M., Nurminen, N., Ylinen, A., 2000. Reciprocal connections between the amygdala and the hippocampal formation, perirhinal cortex, and postrhinal cortex in rat. A review. Ann. NY Acad. Sci. 911, 369–391.

Polymeropoulos, M.H., Swift, R.G., Swift, M., 1994. Linkage of the gene for Wolfram syndrome to markers on the short arm of chromosome 4. Nat. Genet. 8, 95–97.

Price, J.L., Russchen, F.T., Amaral, D.G., 1987. The limbic region. II. The amygdaloid complex. In: Björklund, A., Hökfelt, T., Swanson, L.W. (Eds.), Handbook of Chemical Neuroanatomy. Elsevier, Amsterdam, pp. 279–389.

Rando, T.A., Horton, J.C., Layzer, R.B., 1992. Wolfram syndrome: evidence of a diffuse neurodegenerative disease by magnetic resonance imaging. Neurology 42, 1220–1224.

Ribak, C.E., Vaughn, J.E., Saito, K., 1978. Immunocytochemical localization of glutamic acid decarboxylase in neuronal somata following colchicine inhibition of axonal transport. Brain Res. 140, 315–332.

Risold, P.Y., 2004. The septal region. In: Paxinos, G. (Ed.), The Rat Nervous System. third ed. Elsevier Academic Press, San Diego, pp. 605–632.

Saper, C.B., 2000. Brain stem, reflexive behavior, and the cranial nerves. In: Kandel, E.R., Schwartz, J.H., Jessell, T.M. (Eds.), Principles of Neural Science. fourth ed. McGraw-Hill, New York, pp. 873–888.

Scolding, N.J., Kellar-Wood, H.F., Shaw, C., Shneerson, J.M., Antoun, N., 1996. Wolfram syndrome: hereditary diabetes mellitus with brainstem and optic atrophy. Ann. Neurol. 39, 352–360.

Sefton, A.J., Dreher, B., Harvey, A., 2004. Visual system. In: Paxinos, G. (Ed.), The Rat Nervous System. third ed. Elsevier Academic Press, San Diego, pp. 1083–1165.

Sequeira, A., Kim, C., Seguin, M., Lesage, A., Chawky, N., Desautels, A., Tousignant, M., Vanier, C., Lipp, O., Benkelfat, C., Rouleau, G., Turecki, G., 2003. Wolfram syndrome and suicide: evidence for a role of WFS1 in suicidal and impulsive behavior. Am. J. Med. Genet. B Neuropsychiatr. Genet. 119B, 108–113.

Shannon, P., Becker, L., Deck, J., 1999. Evidence of widespread axonal pathology in Wolfram syndrome. Acta Neuropathol. (Berl.) 98, 304–308.

Shibata, H., 1993. Direct projections from the anterior thalamic nuclei to the retrohippocampal region in the rat. J. Comp. Neurol. 337, 431–445.

Shipley, M.T., Ennis, M., Puche, A.C., 2004. Olfactory system. In: Paxinos, G. (Ed.), The Rat Nervous System. third ed. Elsevier Academic Press, San Diego, pp. 923–964.

Sparsø, T., Andersen, G., Albrechtsen, A., Jørgensen, T., Borch-Johnsen, K., Sandbæk, A., Lauritzen, T., Wasson, J., Permutt, M.A., Glaser, B., Madsbad, S., Pedersen, O., Hansen, T., 2008. Impact of polymorphisms in *WFS1* on prediabetic phenotypes in a population-based sample of middle-aged people with normal and abnormal glucose regulation. Diabetologia 51, 1646–1652.

Strom, T.M., Hörtnagel, K., Hofmann, S., Gekeler, F., Scharfe, C., Rabl, W., Gerbitz, K.D., Meitinger, T., 1998. Diabetes insipidus, diabetes mellitus, optic atrophy and deafness (DIDMOAD) caused by mutations in a novel gene (*wolframin*) coding for a predicted transmembrane protein. Hum. Mol. Genet. 7, 2021–2028.

Swanson, L.W., Köhler, C., Björklund, A., 1987. The limbic region. I. The septohippocampal system. In: Björklund, A., Hökfelt, T., Swanson, L.W. (Eds.), Handbook of Chemical Neuroanatomy. Elsevier, Amsterdam, pp. 125–227.

Swanson, L.W., Wyss, J.M., Cowan, W.M., 1978. An autoradiographic study of the organization of intrahippocampal association pathways in the rat. J. Comp. Neurol. 181, 681–715.

Swift, M., Swift, R.G., 2005. Wolframin mutations and hospitalization for psychiatric illness. Mol. Psychiatry 10, 799–803.

Swift, R.G., Sadler, D.B., Swift, M., 1990. Psychiatric findings in Wolfram syndrome homozygotes. Lancet 336, 667–669.

Takeda, K., Inoue, H., Tanizawa, Y., Matsuzaki, Y., Oba, J., Watanabe, Y., Shinoda, K., Oka, Y., 2001. WFS1 (Wolfram syndrome 1) gene product: predominant subcellular localization to endoplasmic reticulum in cultured cells and neuronal expression in rat brain. Hum. Mol. Genet. 10, 477–484.

Takei, D., Ishihara, H., Yamaguchi, S., Yamada, T., Tamura, A., Katagiri, H., Maruyama, Y., Oka, Y., 2006. WFS1 protein modulates the free Ca^{2+} concentration in the endoplasmic reticulum. FEBS Lett. 580, 5635–5640.

Tamamaki, N., Abe, K., Nojyo, Y., 1987. Columnar organization in the subiculum formed by axon branches originating from single CA1 pyramidal neurons in the rat hippocampus. Brain Res. 412, 156–160.

Taube, J.S., Muller, R.U., Ranck Jr., J.B., 1990. Head-direction cells recorded from the postsubiculum in freely moving rats. I. Description and quantitative analysis. J. Neurosci. 10, 420–435.

Tessa, A., Carbone, I., Matteoli, M.C., Bruno, C., Patrono, C., Patera, I.P., De Luca, F., Lorini, R., Santorelli, F.M., 2001. Identification of novel WFS1 mutations in Italian children with Wolfram syndrome. Hum. Mutat. 17, 348–349.

Travers, J.B., 2004. Oromotor nuclei. In: Paxinos, G. (Ed.), The Rat Nervous System. third ed. Elsevier Academic Press, San Diego, pp. 295–319.

Ueda, K., Kawano, J., Takeda, K., Yujiri, T., Tanabe, K., Anno, T., Akiyama, M., Nozaki, J., Yoshinaga, T., Koizumi, A., Shinoda, K., Oka, Y., Tanizawa, Y., 2005. Endoplasmic reticulum stress induces *Wfs1* gene expression in pancreatic β-cells via transcriptional activation. Eur. J. Endocrinol. 153, 167–176.

Van Groen, T., Wyss, J.M., 1990a. The connections of presubiculum and parasubiculum in the rat. Brain Res. 518, 227–243.

Van Groen, T., Wyss, J.M., 1990b. Extrinsic projections from area CA1 of the rat hippocampus: olfactory, cortical, subcortical, and bilateral hippocampal formation projections. J. Comp. Neurol. 302, 515–528.

Van Groen, T., Wyss, J.M., 1990c. The postsubicular cortex in the rat: characterization of the fourth region of the subicular cortex and its connections. Brain Res. 529, 165–177.

Van Groen, T., Wyss, J.M., 1995. Projections from the anterodorsal and anteroventral nucleus of the thalamus to the limbic cortex in the rat. J. Comp. Neurol. 358, 584–604.

van Groen, T., 2001. Entorhinal cortex of the mouse: cytoarchitectonical organization. Hippocampus 11, 397–407.

Vogt, B.A., Miller, M.W., 1983. Cortical connections between rat cingulate cortex and visual, motor, and postsubicular cortices. J. Comp. Neurol. 216, 192–210.

Vogt, B.A., Vogt, L., Farber, N.B., 2004. Cingulate cortex and disease models. In: Paxinos, G. (Ed.), The Rat Nervous System. third ed. Elsevier Academic Press, San Diego, pp. 705–727.

Waite, P.M.E., 2004. Trigeminal sensory system. In: Paxinos, G. (Ed.), The Rat Nervous System. third ed. Elsevier Academic Press, San Diego, pp. 817–851.

Warr, W.B., de Olmos, J.S., Heimer, L., 1981. Horseradish peroxidase: the basic procedure. In: Heimer, L., Robards, M.J. (Eds.), Neuroanatomical Tract-tracing Methods. Plenum Press, New York, pp. 207–262.

Wasson, J., Permutt, M.A., 2008. Candidate gene studies reveal that the *WFS1* gene joins the expanding list of novel type 2 diabetes genes. Diabetologia 51, 391–393.

Witter, M.P., Amaral, D.G., 2004. Hippocampal formation. In: Paxinos, G. (Ed.), The Rat Nervous System. third ed. Elsevier Academic Press, San Diego, pp. 635–704.

Wolfram, D.J., Wagener, H.P., 1938. Diabetes mellitus and simple optic atrophy among siblings: report of four cases. Mayo Clin. Proc. 13, 715–718.

Wouterlood, F.G., 1991. Innervation of entorhinal principal cells by neurons of the nucleus reuniens thalami. Anterograde PHA-L tracing combined with retrograde fluorescent tracing and intracellular injection with Lucifer yellow in the rat. Eur. J. Neurosci. 3, 641–647.

Wouterlood, F.G., Saldana, E., Witter, M.P., 1990. Projection from the nucleus reuniens thalami to the hippocampal region: light and electron microscopic tracing study in the rat with the anterograde tracer Phaseolus vulgaris-leucoagglutinin. J. Comp. Neurol. 296, 179–203.

Woznicka, A., Malinowska, M., Kosmal, A., 2006. Cytoarchitectonic organization of the entorhinal cortex of the canine brain. Brain Res. Rev. 52, 346–367.

Wyss, J.M., Van Groen, T., 1992. Connections between the retrosplenial cortex and the hippocampal formation in the rat: a review. Hippocampus 2, 1–11.

Yamada, T., Ishihara, H., Tamura, A., Takahashi, R., Yamaguchi, S., Takei, D., Tokita, A., Satake, C., Tashiro, F., Katagiri, H., Aburatani, H., Miyazaki, J., Oka, Y., 2006. WFS1-deficiency increases endoplasmic reticulum stress, impairs cell cycle progression and triggers the apoptotic pathway specifically in pancreatic β-cells. Hum. Mol. Genet. 15, 1600–1609.

Yamaguchi, S., Ishihara, H., Tamura, A., Yamada, T., Takahashi, R., Takei, D., Katagiri, H., Oka, Y., 2004. Endoplasmic reticulum stress and N-glycosylation modulate expression of WFS1 protein. Biochem. Biophys. Res. Commun. 325, 250–256.

Young, T.L., Ives, E., Lynch, E., Person, R., Snook, S., MacLaren, L., Cater, T., Griffin, A., Fernandez, B., Lee, M.K., King, M.C., 2001. Non-syndromic progressive hearing loss *DFNA38* is caused by heterozygous missense mutation in the Wolfram syndrome gene *WFS1*. Hum. Mol. Genet. 10, 2509–2514.

Anal Bioanal Chem (2009) 394:1655–1660
DOI 10.1007/s00216-009-2830-9

ORIGINAL PAPER

Pattern recognition analysis for ^{1}H NMR spectra of plasma from hemodialysis patients

Masako Fujiwara · Takeshi Kobayashi · Takahiro Jomori · Yutaka Maruyama · Yoshitomo Oka · Hiroshi Sekino · Yutaka Imai · Kazuhisa Takeuchi

Received: 9 March 2009 / Revised: 28 April 2009 / Accepted: 30 April 2009 / Published online: 1 June 2009

Abstract ^{1}H NMR spectroscopic and pattern recognition-based methods (NMR-PR) were applied to the metabolic profiling studies on hemodialysis (HD). Plasma samples were collected from 37 patients before and after HD and measured by 600 MHz NMR spectroscopy. Each spectrum was data-processed and subjected to principal component analysis for pattern recognition. Spectral patterns of plasma between pre- and post-dialyses were clearly discriminated, together with significant fluctuations in the levels of creatinine, trimethylamine-*N*-oxide, glucose, lactate, and acetate, which were quantitated. We have first observed the significant elevation of lactate levels in post-dialysis plasma. The present study has demonstrated the high feasibility of NMR-PR method for monitoring the dialysis condition and comprehensive profiling of the change of low-molecular-weight metabolites in HD.

Keywords Lactate · Acetate · TMAO · PCA · Renal failure · Metabolomics

M. Fujiwara (✉) · T. Kobayashi · Y. Imai · K. Takeuchi
Graduate School of Pharmaceutical Sciences, Tohoku University,
6-3, Aramaki-aza-aoba, Aoba-ku,
Sendai 980-8578, Japan
e-mail: fmasako@m.tains.tohoku.ac.jp

T. Jomori
Faculty of Pharmaceutical Sciences, Tohoku University,
Sendai, Japan

M. Fujiwara · Y. Maruyama · Y. Imai
The Tohoku University 21st Century COE Program
"CRESCENDO",
Sendai, Japan

Y. Oka
Division of Molecular Metabolism and Diabetes,
Graduate School of Medicine, Tohoku University,
Sendai, Japan

H. Sekino · K. Takeuchi
CKD Center, Koujinkai Central Hemodialysis Clinic,
Sendai, Japan

Present Address:
Y. Maruyama
Department of Career Development, Seiwa Gakuen College,
Sendai, Japan

Introduction

NMR spectroscopy of biofuilds has introduced a new chemistry analysis tool to life science and clinical medicine with the high filed NMR spectrometers [1]. The technique has been applied to various disease characterization and diagnostic or prognostic researches on cardiovascular diseases [2], cancer [3], inborn errors of metabolism [4], diabetes [5, 6], arthritis [7], liver disease [8], etc. [9]. The studies on renal failure [10–13] and HD therapy [14] have been performed as well. The previous metabolomic study using ^{1}H NMR spectroscopy in HD patients under the HD buffer containing acetate showed an accumulation of acetate and metabolism during the course of the dialysis and demonstrated changes in the relative concentrations of endogenous plasma components [15]. A subsequent ^{1}H, ^{13}C, and ^{14}N NMR study of the plasma and urine from renal failure patients showed that the plasma levels of TMAO (trimethylamine-*N*-oxide) correlated with those of urea and creatinine, suggesting that the presence of TMAO is closely related to the degree of renal failure [16]. In these studies, however, the subject number was limited.

NMR metabolomics combined with multivariate pattern recognition would give an advantage over other conventional

analyses. The method of principal component analysis (PCA) simplifies the multivariate data into two or three dimensions that can be readily understood and evaluated [17]. This analysis allows one to discriminate between different subgroups existent in the total population by their characteristic patterns of spectra [18, 19]. It is also possible to identify the relevant biomarkers [20]. PCA does not require any identification of signals but the processed numerical data from spectra intensity (non-targeted analysis) [21]. The score plot can depict classification of groups by the characteristic of spectral patterns [22].

The purpose of our study was to assess the utility of ^{1}H NMR metabolomics using pattern recognition analysis of plasma in HD. In the present study, plasma from 37 patients were measured by ^{1}H NMR spectroscopy and subjected to PCA. The analysis has revealed some metabolites behaviors: elevation of acetate, glucose, and lactate in post-dialysis plasma, of which levels were quantitated by ^{1}H NMR spectroscopy.

Methods

Patients Thirty-seven patients had been studied. After the approval of the study protocol by the ethical committee (Koujinkai Central Hemodialysis Clinic, Sendai, Japan), informed consents have been obtained. The characteristic were age between 39 and 93 years; gender, 48% women; and cause of renal failure, diabetic nephropathy diabetes mellitus 34%, chronic glomerulonephritis or nephropathy 34%, and others (nephrosclerosis, congenital renal disease, etc.). Their hemodialysis conditions were stable, and the duration of hemodialysis was between 2 and 32 years (average, 10.5 years). Their metabolic findings such as levels of blood glucose and lipids were not significantly different in the patients.

Samples Venous blood samples from subjects undergoing HD using bicarbonate dialysis buffers (containing acetate of 8–12 mM and glucose of 5–8 mM) were collected into lithium heparin tubes. After centrifuging, the plasma was stored at −20 °C. It was thawed at room temperature immediately before use, and any precipitation was removed by centrifugation. For NMR, 200 µl of plasma and 400 µl so-called NMR cocktail (saline with 5 mM TSP (sodium 3-(trimethylsilyl) propionic 2, 2, 3, 3-d_4) as both concentration and chemical shift reference, NaN_3 for preventing and D_2O 50 µl for the internal field-frequency lock) was placed into 5-mm NMR tube.

NMR spectroscopy Single-pulse ^{1}H NMR spectra were recorded at 35 °C internal probe temperature using 600 MHz NMR spectrometer (JEOL ECA) quipped with a sample changer. Each spectrum consisted of 64 K complex data points with a spectrum width 6 kHz, where each spectrum was accumulated by 64 scans with an acquisition time of 1.75 s and a recycle delay of 5 s per scan. The detection pulse flip angle was set to 45°. A pre-saturation sequence was used to suppress the water signal.

NMR data reduction procedures Each NMR spectrum was segmented into 225 regions of 0.04 ppm width over the range of 0.5 to 9.5 ppm, and each segment of the spectral regions was integrated. Integrated regions from 4.3 to 5.2 ppm, which contained residual water resonance, were eliminated from the data table, and then data were reduced to 202 variable regions. The remaining integral values of each spectrum were normalized for 100 of the total summed integrals in order to compensate for any differences of the plasma samples. These processing and successive PCA was performed by ALICE2 for Metabolome® software package (version 1.0; JEOL, Tokyo, Japan).

Quantitation of metabolites Serial additions of lactate (0.5, 1.0, 1.5, 2.0, 3.0, and 5.0 mM) were performed to the randomly selected three-paired samples of pre- and post-plasma. Every result of six experiments exhibited the linear relation between the signal area of each addition and the concentration lactate added. The chemical shift and line-width did not change on each experiment. The sensitivity of signal area vs. concentration was not exactly same in each sample. However, six sensitivities revealed to be within ±10% deviation from the average. In the present study, the practical approximation was applied for use of this average sensitivity to calibrate the absolute lactate concentration of signal areas. The values of concentrations for glucose and acetate were calculated in the same way by using corresponding proton numbers [15].

Results

Metabolic profiling by ^{1}H NMR

Figure 1 shows the representative plasma spectra of pre- and post-dialysis using bicarbonate buffer containing acetate and the spectrum of initial waste fluid from dialyser. In Fig. 1a of the pre-dialysis spectrum, the resonances of methyl (3.04 ppm) and methylene (4.05 ppm) of creatinine and methyls (3.28 ppm) of TMAO were significantly increased comparative with that of post-dialysis in which acetate (1.92 ppm) signal appeared [23]. Glucose exhibited many sharp signals between creatinine peaks in both spectra in Fig. 1a and b. Every pre-dialysis spectrum had little signal of acetate. The waste solution measured was taken 15 min after the start of dialysis treatment, and the spectrum exhibited not only signals of acetate and glucose

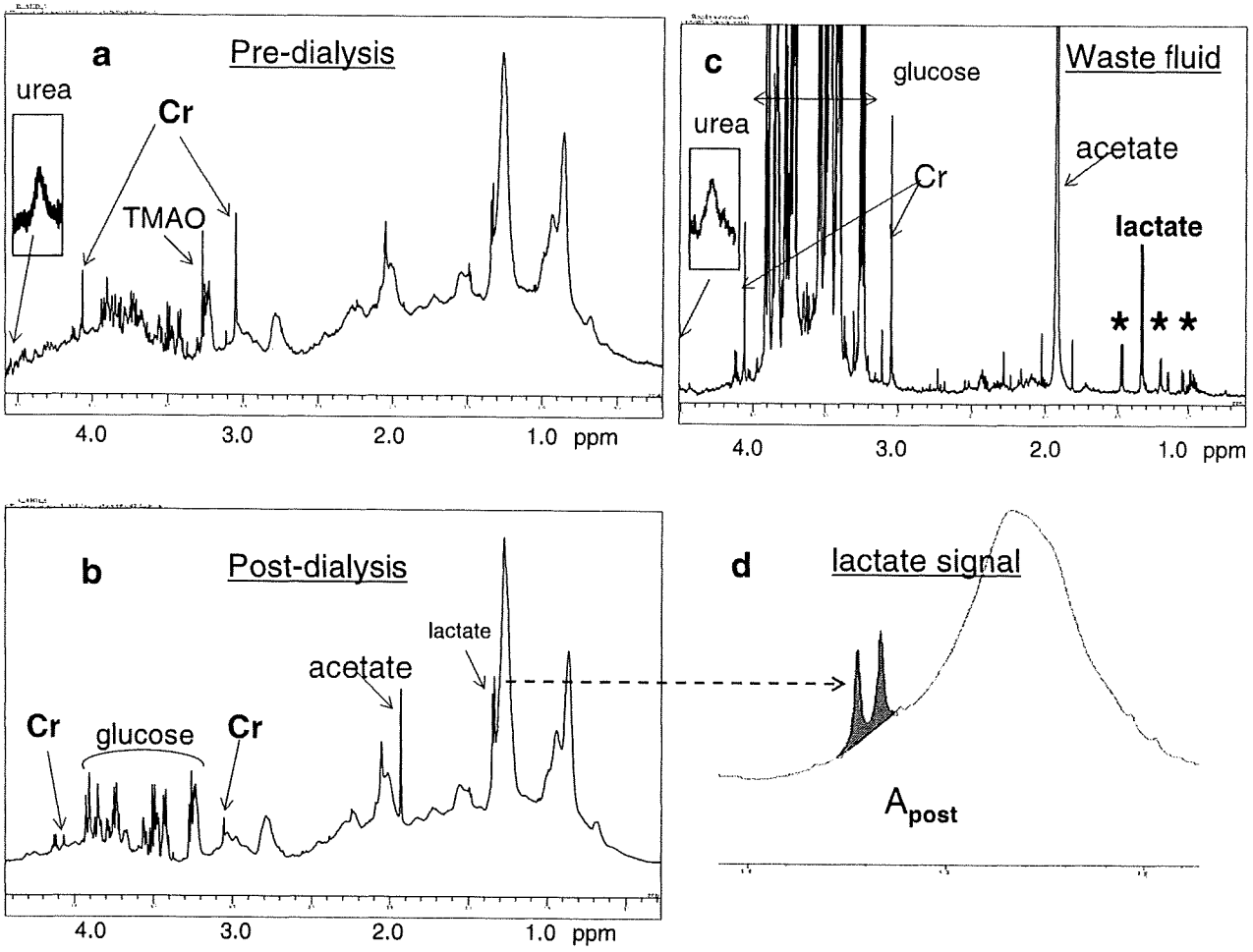

Fig. 1 ^{1}H NMR spectra (600 MHz) of plasma from pre- and post-dialysis (**a**, **b**) and of waste fluid (**c**) in the higher field, respectively. Cr indicates creatinine signal. In each spectra (**a**, **c**), there was a signal of urea at 5.78 ppm inserted to the figure with enlargement, respectively. In **c**, the *asterisk-marked* signals indicate valine, threonine, and alanine from the right, respectively. **d** The enlargement of lactate signal. The signal areas, A_{post} and A_{pre}, were measured after adequate baseline correction indicated as a *shaded area*, respectively, and used for calculation of Δ

in dialysate fluid constituents but also those of creatinine, lactate, amino acids, and organic acids that were filtered out of plasma already.

^{1}H NMR spectra of 37 pairs (pre- and post-dialysis plasma) were measured and processed as mentioned above and submitted to PCA. As shown in Fig. 2a, the two groups were clearly separated. The PC1 axis successfully extracted dialysis effect dominantly. Loading plot is shown in Fig. 2b; the distribution of variables corresponds to that of samples in score plot. The lower group reflects the increase level of acetate; samples of right side have larger signals of lipid so on. Figure 2c shows distribution of contribution of variables to PCs; every bar (variable) consists of contributions to PC1 (red), PC2 (blue), PC3 (green), and the residuals (cyan). The variables of lipid and glucose in Fig. 2c have large contribution to PC2, which corresponds to PC2, i.e., the horizontal axis of score plot in Fig. 2a. The variable of 3.28 ppm (TMAO) has the big contribution to PC3 nearly the same ratio as that to PC1.

Figure 2d showed also the loading depicted in the cross-sectional graph of Fig. 2b along PC1 axis. This profile of all the metabolites was responsible for making PC1 axis to characterize and discriminate the two groups. The upper bars, including creatinine, TMAO, threonine, alanine, etc., are large in the upper group samples (pre-), and the lower bars, including glucose, acetate, and lactate, are large in the lower group samples (post-) in Fig. 2a, respectively. This figure illustrates the quantitative fluctuation of all the metabolites simultaneously. The lower big bar of acetate and glucose were considered to be derived from dialysis fluid constituents; however, elevated post-plasma level of lactate was unexpectedly observed.

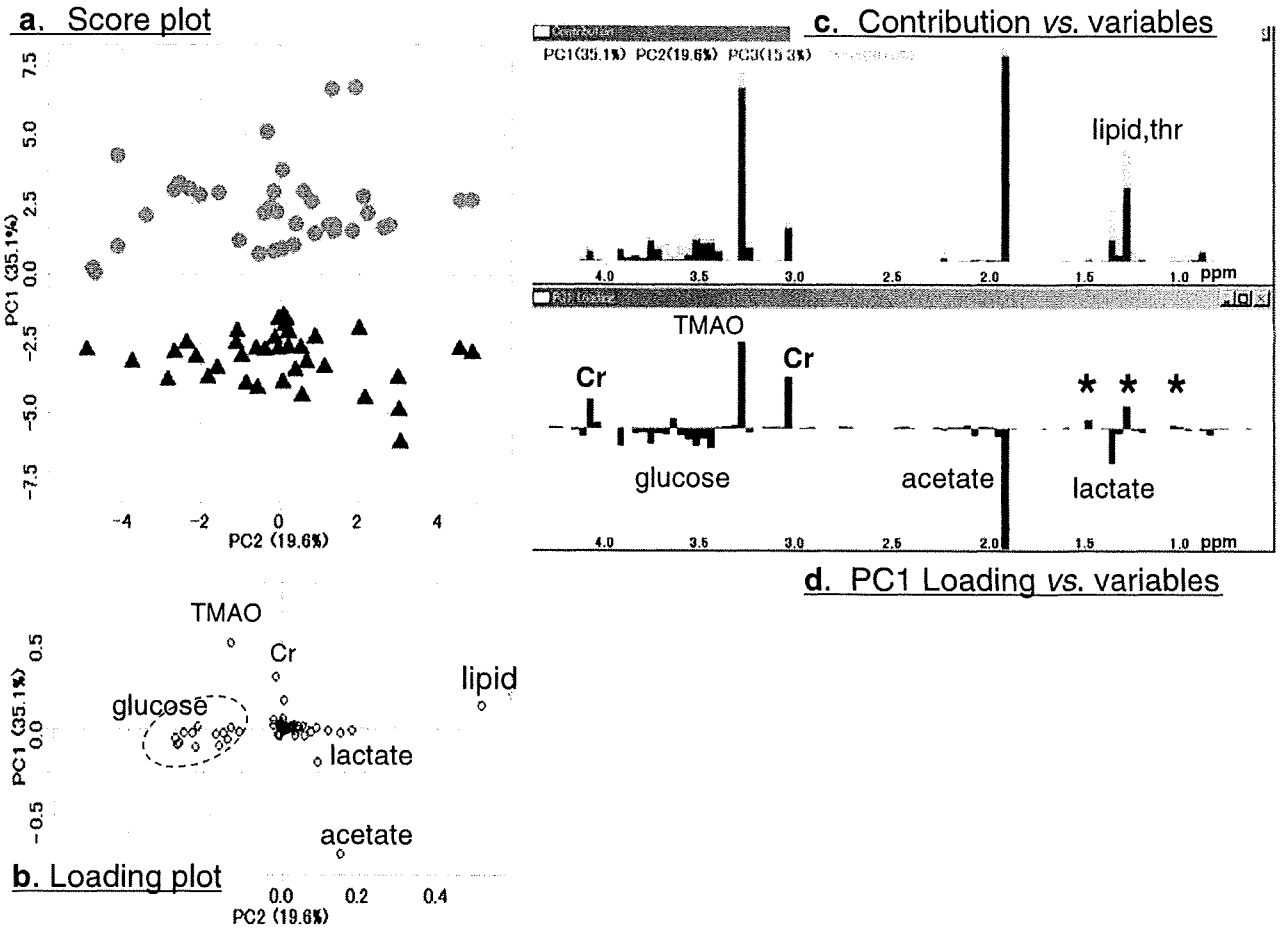

Fig. 2 **a** PCA score plot of PC1-PC2; *orange circle* and *purple triangle dots* indicate spectra from pre- and post-dialysis subjects, respectively. PC1 and PC2 explained 31.5% and 19.8% of total variance, respectively. **b** Loading plot; major metabolites were indicated. **c** Contribution quantities of variables in higher field showing that responsible for PCA classification. The *red*, *blue*, *green*, and *cyan bars* correspond to the contribution to PC1, PC2, PC3, and the residuals, respectively. **d** A plot of PC1 loading vs. variables. The *asterisk-marked* variables are valine, threonine, and alanine corresponding to Fig. 1

Quantitation of creatinine, TMAO, acetate, glucose, and lactate

For further investigation, we tried to quantify metabolites that changed greatly, creatinine, TMAO, acetate, glucose, and lactate, between pre- and post-treatment.

We have quantitated by integration of signal areas from small metabolites [24] after adequate baseline correction like as in Fig. 1d. For the quantitation of differences between pre- and post-resonances of the metabolites, the subtraction pre-signal area A_{pre} from post-signal area A_{post}, that is, $\Delta = A_{post} - A_{pre}$, was calculated for each paired

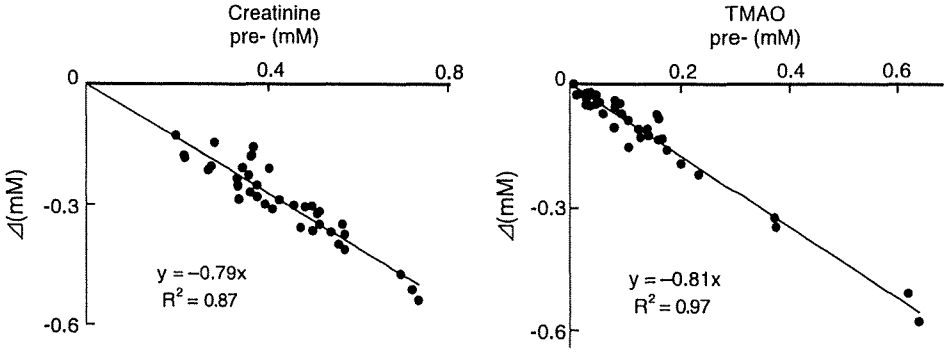

Fig. 3 Correlation of the concentration between pre- and difference of 37 subjects in mM, respectively. A *red line* indicates 0 value of Δ on each graph. Linear regression line was depicted on graphs of creatinine and TAMO

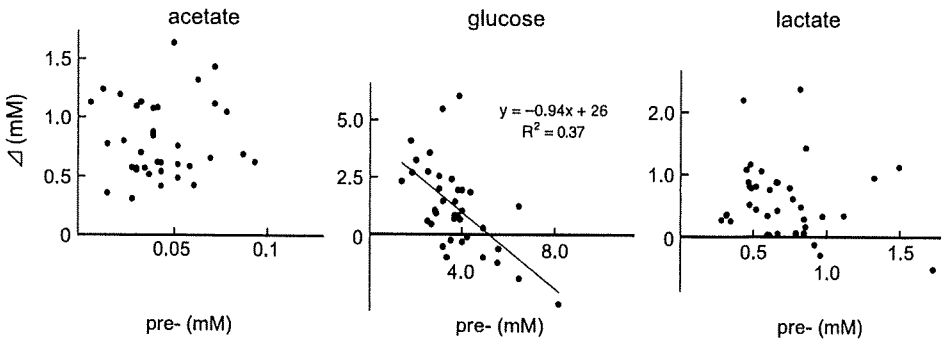

Fig. 4 Correlations of concentration between pre- and difference of 37 subjects for acetate, glucose, and lactate, in mM, respectively. A *red line* indicates 0 value of Δ on each graph

spectra. We determined graded several concentrations of lactate added to samples for the transformation signal areas to concentration, as mentioned in the previous section. Thus, the concentrations of pre-dialysis vs. the difference (Δ) for metabolites of 37 were plotted in mM in Figs. 3 and 4.

In Fig. 3, differences of creatinine and TMAO were revealed to have all negative values, which show successful clearance by dialysis, and to be greatly dependent upon the initial accumulated values of each. The linear regression graphs showed the following relation,

$$\Delta = A_{post} - A_{pre} \fallingdotseq -0.8\, A_{pre}$$

Then $A_{post} \fallingdotseq 0.2\, A_{pre}$

Values of post- became 1/5 that of pre-; it meant the treatment cleared 80% of accumulated ureic toxins.

As shown in Fig. 4, the differences (Δ) of acetate showed all positive values with much variance, that of glucose presented mostly positive values with a negative correlation to its pre- values, and the most values of that for lactate were significantly positive with much variance. These concentrations of average and maximum of all 37 samples were summarized in Table 1.

Discussion

NMR method requires little or no pretreatment of the sample, and it allows a simultaneous quantitation of metabolites in a spectrum [15]. NMR-PR method has no specific target metabolites to be analyzed but it reveals whole spectral pattern, and therefore, the statistical analysis of PCA leads to comprehensive profile, including not only creatinine, TMAO, glucose, and acetate but also lactate and others. The present analysis clearly extracted the balance change.

We have showed that creatinine, TMAO, alanine, thereonine, and other low-molecule metabolites were cleared from plasma by dialysis, while acetate, glucose, and lactate levels were elevated in post-dialysis plasma. TMAO accumulation in the end-stage-kidney disease [16] and its clearance by dialysis have already been reported [25]. We here observed a weak correlation between pre-dialysis plasma levels of TMAO and creatinine, although the levels of TMAO vary, probably depending on the amount of dietary intake which digest TMAO, such as fish meat [24]. The dialysate constituents could cause acetate level increment, as expected. The variance of Δ acetate values shown in Fig. 4 was due to individual variety. As for glucose, the values were varied probably due to the balance between the plasma levels of glucose and dialysis buffer or the meal intake during HD

In the post-HD, plasma levels of lactate were significantly increased. There has been no report on the observation. As shown in Fig.1c, lactate is a small molecule to be filtered continuously with the same ratio as creatinine and TMAO; the increment plasma level of lactate (its average of 0.7 mM as shown in Table 1) was due to a de novo synthesis during HD. The cause of lactate increase is unknown. In HD, dehydration would lower blood perfusion to tissues, leading to the peripheral hypoxemia resulting in anaerobic glycolysis causing lactate synthesis, or the change of pH during HD may influence the degradation of lactate by lactate dehydrogenase [26].

In conclusion, NMR-PR method has promising scope for a monitoring HD treatment together with comprehensive and visual metabolic profiling.

Table 1 The values of mean and maximum of 37 samples (mM)

		mean±SD	max
lactate	pre	0.9±0.4	2.1
	post	1.6±0.6	3.9
	Δ	0.7±0.6	1.8
glucose	pre	3.6±1.4	7.9
	post	4.9±1.6	10.5
	Δ	1.3±2.0	6.6
acetate	pre	0.04±0.02	0.1
	post	0.9±0.3	1.7
	Δ	0.8±0.3	1.6

Acknowledgment This work was supported in part by Grants-in-Aid from the Ministry of Education, Culture, Sports, Science and Technology of Japan (19590930, 20659004) and a grant from Kirin Pharm. Co. Ltd.

References

1. Nicholson JK, Wilson ID (1989) High resolution proton magnetic resonance spectroscopy of biological fluids. Prog Nucl Magn Reson Spectrosc 21:449–551
2. Brindle JT, Antti H, Holmes E, Tranter G, Nicholson JK, Bethell HW, Clarke S, Schofield PM, McKilligin E, Mosedale DE, Grainger DJ (2002) Rapid and noninvasive diagnosis of the presence and severity of coronary heart disease using ^{1}H NMR-based metabolomics. Nat Med 8:1430–1444
3. Chen LL, Burns MA, Taylor JL, HE W, Halpern EF, McDougal WS, Wu CL (2005) Metabolic characterization of human prostate cancer with tissue magnetic resonance spectroscopy. Cancer Res 65:3030–3034
4. Moonlenaar SH, Engelke UF, Wevers RA (2003) Proton nuclear magnetic resonance spectroscopy of body fluids in the field of inborn errors of metabolism. Ann Clin Biochem 40:16–24
5. Nicholson JK, O'Flynn MP, Sadler PJ, Macleod AF, Juul SM (1984) Proton-nuclear-magnetic-resonance studies of serum, plasma, and urine from fasting normal and diabetic subjects. Biochem J 217:365–375
6. Makinen V-P, Soininen P, Forsblom C, Parkonen M, Ingman P, Kaski K, Groop P-H, Ala-Korpela M (2008) ^{1}H NMR metabonomics approach to disease continuum of diabetic complications and premature death. Mol Syst Biol 4:1–11
7. Parkers HG, Grootveld M, Henderson EB, Farrell A, Blake DR (1991) Oxidative damage to synovial fluid from the inflamed rheumatoid joint detected by ^{1}H NMR spectroscopy. J Pharm Biomed Anal 9:75–82
8. Clayton TA, Lindon JC, Everett JR, Charuel C, Hanton G, Net LJ-L, Provost J-P, Nicholson JK (2004) Hepatotoxin-induced hypercreatinaemia and hypercreatinuria: their relationship to one another, to liver damage and to weakened nutritional status. Arch Toxicol 78:86–96
9. Lindon JC, Holmes E (2007) A survey of metabolomics approaches for disease characterization. In: Lindon JC et al (ed) The handbook of metabonomics and metabolomics. Elsevier B. V., Amsterdam, pp. 427–434
10. Knubovets TL, Lundina TA, Sibeldina LA, Sedov KR (1992) ^{1}H NMR urinalysis in glomerulopheritis: a new prognostic criterion. Magn Reson Imaging 10:127–134
11. Holmes E, Foxall PJD, Nicholson JK (1990) Proton NMR analysis of plasma from renal failure patients: Evaluation of sample preparation and spectral-editing method. J Pharm Biomed Anal 8:955–958
12. Foxall PJD, Spraul M, Farrant RD, Lindon JC, Nicholson JK (1993) 750 MHz ^{1}H NMR spectroscopy of human blood plasma. J Pharm Biomed Anal 11:267–276
13. Foxall PJD, Price RG, Jones JK, Neild GH, Tompson FD, Nicholson JK (1992) High resolution proton magnetic resonance spectroscopy of cyst fluid from patients with polycystic kidney disease. Biochem Biophys Acta 1138:305–314
14. Scholze A, Jankowski V, Henning L, Haass W, Wittstock A, Suvd-Erdene S, Zidek W, Tepel M, Jankowski J (2007) Phenylacetic acid and arterial vascular properties in patients with chronic kidney disease stage 5 on hemodialysis therapy. Nephron Clin Pract 107:1–6
15. Grasdalen H, Belton PS, Pryor JA, Rich GT (1987) Quantitative proton magnetic resonance of plasma from uraemic patients during dialysis. Magn Reson Chem 25:811–816
16. Bell JD, Lee A, Lee HA, Sadler PJ, Wdkle DR, Woodhaml RH (1991) Nuclear magnetic resonance studies of blood plasma and urine from subjects with chronic renal failure: identification of trimethylamine-N-oxide. Biochemica et Biophysica Acta 1096:101–107
17. Xu L (ed) (1995) Methods of chemometrics. Science, Beijing
18. Holmes E, Nicholls AW, Lindon JC, Ramos S, Spraul M, Neidig P, Connor SC, Connelly J, Damment SJP, Haselden J, Nicholson JK (1998) Developing of a model for classification of toxin-induced lesions using ^{1}H NMR spectroscopy of urine combined with pattern recognition. NMR Biomed 11:235–244
19. Fujiwara M, Ando I, Arifuku K, Nemoto T (2005) Pattern recognition analysis for classification of hypertensive model rats and diurnal variation using ^{1}H-NMR spectroscopy of urine. Anal Sci 21:1259–1262
20. Duarte IF, Goodfellow BJ, Barros A, Jones JG, Barosa C, Diogo L, Garcia P, Gil AM (2007) Metabolic characterization of plasma in juveniles with glycogen storage disease type 1a (GSD1a) by high-resolution ^{1}H NMR spectroscopy. NMR Biomed 20:401–412
21. Nemoto T, Ando I, Kataoka T, Arifuku K, Kanazawa K, Natori Y, Fujiwara M (2007) NMR metabolic profiling combined with two-step principal component analysis for toxin-induced diabetes model rat using urine. J Toxicol Sci 32:429–435
22. Maher AD, Zirah SFM, Holmes E, Nicholson JK (2007) Experimental and analytical variation in human urine in ^{1}H NMR spectroscopy-based metabolic phenotyping studies. Anal Chem 79:5204–5211
23. Nicholson JK, Foxall PJD (1995) 750 MHz ^{1}H and ^{1}H–^{13}C NMR spectroscopy of human blood plasma. Anal Chem 67:793–811
24. Maschke S, Wahl A, Azaroual N, Boulet O, Crunelle V, Imbenotte M, Foulard M, Vemeersch G, Lhermitte M (1997) ^{1}H NMR analysis of trimethylamine in urine for the diagnosis of fish-odour syndrome. Clin Chim Acta 263:139–146
25. Bain MA, Faull R, Fornasini G, Milne RE, Evans AM (2006) Accumulation of trimethylamine and trimethylamine-*N*-oxide in end-stage-renal disease patients undergoing haemodialysis. Nephrol Dial Transplant 21:1300–1304
26. Bellomo R (2002) Bench-to-bedside review: lactate and the kidney. Crit Care 6:322–326

Journal of Human Genetics (2009) 54, 236–241

www.nature.com/jhg

ORIGINAL ARTICLE

Construction of a prediction model for type 2 diabetes mellitus in the Japanese population based on 11 genes with strong evidence of the association

Kazuaki Miyake[1], Woosung Yang[2], Kazuo Hara[3], Kazuki Yasuda[4], Yukio Horikawa[5], Haruhiko Osawa[6], Hiroto Furuta[7], Maggie CY Ng[8], Yushi Hirota[1], Hiroyuki Mori[1], Keisuke Ido[2,20], Kazuya Yamagata[9,21], Yoshinori Hinokio[10], Yoshitomo Oka[10], Naoko Iwasaki[11], Yasuhiko Iwamoto[11], Yuichiro Yamada[12,22], Yutaka Seino[12,23], Hiroshi Maegawa[13], Atsunori Kashiwagi[13], He-yao Wang[4,24], Toshihito Tanahashi[14], Naoto Nakamura[15], Jun Takeda[5], Eiichi Maeda[2], Ken Yamamoto[16], Katsushi Tokunaga[17], Ronald CW Ma[8], Wing-Yee So[8], Juliana CN Chan[8], Naoyuki Kamatani[18], Hideichi Makino[6], Kishio Nanjo[7], Takashi Kadowaki[3] and Masato Kasuga[1,19]

Prediction of the disease status is one of the most important objectives of genetic studies. To select the genes with strong evidence of the association with type 2 diabetes mellitus, we validated the associations of the seven candidate loci extracted in our earlier study by genotyping the samples in two independent sample panels. However, except for *KCNQ1*, the association of none of the remaining seven loci was replicated. We then selected 11 genes, *KCNQ1*, *TCF7L2*, *CDKAL1*, *CDKN2A/B*, *IGF2BP2*, *SLC30A8*, *HHEX*, *GCKR*, *HNF1B*, *KCNJ11* and *PPARG*, whose associations with diabetes have already been reported and replicated either in the literature or in this study in the Japanese population. As no evidence of the gene–gene interaction for any pair of the 11 loci was shown, we constructed a prediction model for the disease using the logistic regression analysis by incorporating the number of the risk alleles for the 11 genes, as well as age, sex and body mass index as independent variables. Cumulative risk assessment showed that the addition of one risk allele resulted in an average increase in the odds for the disease of 1.29 (95% CI=1.25–1.33, $P=5.4\times10^{-53}$). The area under the receiver operating characteristic curve, an estimate of the power of the prediction model, was 0.72, thereby indicating that our prediction model for type 2 diabetes may not be so useful but has some value. Incorporation of data from additional risk loci is most likely to increase the predictive power.
Journal of Human Genetics (2009) **54**, 236–241; doi:10.1038/jhg.2009.17; published online 27 February 2009

Keywords: gene–gene interaction; genome-wide association study; prediction model; single nucleotide polymorphism (SNP); type 2 diabetes mellitus

[1]Division of Diabetes, Metabolism and Endocrinology, Department of Internal Medicine, Kobe University Graduate School of Medicine, Kobe, Japan; [2]Clinical Genome Informatics Center, Kobe University Graduate School of Medicine, Kobe, Japan; [3]Department of Metabolic Diseases, Graduate School of Medicine, University of Tokyo, Tokyo, Japan; [4]Department of Metabolic Disorder, Research Institute, International Medical Center of Japan, Tokyo, Japan; [5]Division of Molecule and Structure, Department of Diabetes and Endocrinology, Gifu University School of Medicine, Gifu, Japan; [6]Department of Molecular and Genetic Medicine, Ehime University Graduate School of Medicine, Ehime, Japan; [7]First Department of Medicine, Wakayama Medical University, Wakayama, Japan; [8]Department of Medicine and Therapeutics, The Chinese University of Hong Kong, Shatin, Hong Kong; [9]Department of Metabolic Medicine, Graduate School of Medicine, Osaka University, Osaka, Japan; [10]Division of Molecular Metabolism and Diabetes, Tohoku University Graduate School of Medicine, Sendai, Japan; [11]Department of Medicine, Diabetes Center, Tokyo Women's Medical University, Tokyo, Japan; [12]Department of Diabetes and Clinical Nutrition, Kyoto University School of Medicine, Kyoto, Japan; [13]Division of Endocrinology and Metabolism, Department of Medicine, Shiga University of Medical Science, Shiga, Japan; [14]Division of Genetic Information, Institute for Genome Research, University of Tokushima, Tokushima, Japan; [15]Department of Endocrinology and Metabolism, Kyoto Prefectural University of Medicine, Graduate School of Medical Sciences, Kyoto, Japan; [16]Department of Molecular Genetics, Medical Institute of Bioregulation, Kyushu University, Fukuoka, Japan; [17]Department of Human Genetics, Graduate School of Medicine, University of Tokyo, Tokyo, Japan; [18]Division of Genomic Medicine, Department of Advanced Biomedical Engineering and Science, Tokyo Women's Medical University, Tokyo, Japan and [19]Research Institute, International Medical Center of Japan, Tokyo, Japan

Correspondence: Dr M Kasuga, Research Institute, International Medical Center of Japan, 1-21-1 Toyama, Shinjuku-ku, Tokyo 162-8655, Japan.
E-mail: kasuga@ri.imcj.go.jp

[20]Current address: Information Center for Medical Sciences, Tokyo Medical and Dental University, Tokyo, Japan.
[21]Current address: Faculty of Medical and Pharmaceutical Sciences, Department of Medical Biochemistry, Kumamoto University, Kumamoto, Japan.
[22]Current address: Department of Internal Medicine, Akita University School of Medicine, Akita, Japan.
[23]Current address: Kansai Electric Power Hospital, Osaka, Japan.
[24]Current address: Shanghai Institute of Materia Medica, Chinese Academy of Science, Shanghai, China.
Received 22 December 2008; revised 25 January 2009; accepted 5 February 2009; published online 27 February 2009

INTRODUCTION

Genome-wide association studies (GWASs) have identified novel susceptibility genes for type 2 diabetes mellitus in Caucasians.[1–5] *TCF7L2*, *CDKAL1*, *CDKN2A/B*, *IGF2BP2*, *SLC30A8* and *HHEX* have been widely replicated as susceptibility genes for type 2 diabetes in Asian populations[6–12] as well as in populations of European ancestry.[13,14] We recently identified *KCNQ1* as a novel susceptibility gene, as well as seven other candidate susceptibility loci in a multistage GWAS for type 2 diabetes in the Japanese population, in which a total of 1612 cases and 1424 controls and 100 000 single nucleotide polymorphisms (SNPs) were included.[15] *KCNQ1* was found to confer risk of type 2 diabetes with a relatively large effect size in Asian populations (odds ratio (OR) for Japanese, Chinese and Korean individuals of 1.42),[15] which was similar to that demonstrated earlier for *TCF7L2* in the Japanese population.[6]

Follow-up of GWASs includes analysis of second-tier genes, meta-analysis for specific populations, as well as analysis of gene–gene or gene–environment interactions. A large-scale meta-analysis[16] and an analysis of gene–gene interaction for susceptibility genes[17] have been performed for type 2 diabetes in populations of European ancestry.

In this study, we attempted to confirm in independent subject panels of Japanese and Hong Kong Chinese individuals the associations of the seven candidate susceptibility loci that we identified in addition to *KCNQ1* in our GWAS of type 2 diabetes.[15] However, as described in this article, we failed to replicate the associations of the seven loci with diabetes. We then attempted to extract genes with strong evidence of the associations with diabetes, and selected 11 genes, including *KCNQ1*. As we did not detect any gene–gene interaction between the 11 genes, we then attempted to construct a prediction model for this disease by using the data from the 11 genes, as well as age, gender and body mass index (BMI) as independent variables to obtain a comprehensive understanding of the genetic background of diabetes in the Japanese population.

MATERIALS AND METHODS

Validation of the results from a multistage GWAS in the Japanese population

Study subjects. We assembled two independent subject panels for our replication study: replication-Japanese and replication-Chinese. The 1000 cases and 1000 controls for the replication-Japanese panel were recruited by the Study Group of the Millennium Genome Project for Diabetes Mellitus. The inclusion criteria for diabetic patients were (i) an age at disease onset of 30–60 years and (ii) the absence of antibodies to GAD. Types of diabetes other than type 2 were excluded on the basis of clinical data. The criteria for controls included (i) an age of >50 years, (ii) no past history of a diagnosis of diabetes and (iii) an HbA_{1c} content of <5.8%.

For the replication-Chinese panel, subjects of southern Han Chinese ancestry, who resided in Hong Kong, were recruited. The cases consisted of 1416 individuals with type 2 diabetes selected from the Prince of Wales Hospital Diabetes Registry;[5,18] 626 of these subjects had early-onset diabetes (age at diagnosis of <40 years) and a positive family history, whereas the remaining 790 patients were randomly selected from the registry. Patients with classic type 1 diabetes with acute ketotic presentation or a continuous requirement for insulin within 1 year of diagnosis were excluded. The controls consisted of 1577 subjects with normal glucose tolerance (fasting plasma glucose concentration of <6.1 mmol l^{-1}); 596 of these individuals were recruited either from the general population participating in a community-based screening program for cardiovascular risk or from hospital staff, whereas the remaining 981 subjects were recruited from a population-based screening program for cardiovascular risk in adolescents.[19] The clinical characteristics of the subjects in each panel are summarized in Supplementary Table 1A. The study protocol was approved by the local ethics committee of each institution. Written informed consent was obtained from each subject.

Study design and statistical analysis. For the validation of the results from our earlier multistage GWAS,[15] seven SNPs (rs2250402, rs2307027, rs3741872, rs574628, rs2233647, rs3785233 and rs2075931) were genotyped in the two panels either by sequence-specific primer–PCR analysis followed by fluorescence correlation spectroscopy[20] or by real-time PCR analysis with TaqMan probes (Applied Biosystems, Foster City, CA, USA). Differences in allele frequency between cases and controls for each SNP were evaluated by χ^2 with one degree of freedom. Meta-analysis was performed by the Mantel–Haenszel method (fixed-effects models) with the 'meta' package of the R-Project (http://www.r-project.org). A *P*-value of <0.05 was considered statistically significant.

Examination of gene–gene interaction and construction of a prediction model

Study subjects. In total, 2424 cases and 2424 controls of the Japanese population obtained by combining the second and third screening panels in our original study[15] and the replication-Japanese panel of this study were included in this analysis (analysis-panel). The criteria for the second and third screening panels were described in the earlier report.[15] The clinical characteristics of the subjects are summarized in Supplementary Table 1B.

Selection of the loci included in this study. Prediction of the phenotypes on the basis of genetic polymorphisms should include the genetic data from the loci with strong evidence of the association. Starting from 15 genes described in earlier reports, we selected 11 genes with strong evidence of the association on the basis of the data in the literature and on the results of the replication experiments in this study. Process of the selection of the 11 genes will be described in detail in Results.

Statistical methods. Multiplicative gene–gene interaction was evaluated for each pair of the 11 genes using an interaction term in addition to the terms for the pair of the genes in the logistic regression model. The genotypes for each locus were coded by 0, 1 and 2. Correction for multiple testing was performed by Bonferroni's method.

As there was no evidence for the presence of gene–gene interactions, we attempted to construct a phenotype prediction model by incorporating the number of risk alleles for the 11 loci as an independent variable in addition to age, gender and BMI. The Cochran–Armitage test was used to examine the trend of the increase in the odds by increasing the number of the risk alleles. To construct a prediction model, the log of odds was expressed by the linear combination of the independent variables. Coefficients for the variables were estimated by the logistic regression analysis after making disease (cases) or nondisease (controls) as the dependent variable. Using the coefficients estimated by the logistic regression analysis, we constructed a phenotype prediction model. To evaluate the prediction model, receiver operating characteristic (ROC) curves[21] for the sensitivity and specificity of the prediction model with or without adjustment for age, sex and BMI were generated, and the area under the curve (AUC) was calculated from the ROC curve.

RESULTS

Validation of the results from a multistage GWAS in the Japanese population

We identified earlier 10 loci associated with type 2 diabetes by three-staged GWAS starting from 100 000 SNPs. Among the 10 loci, 3 SNPs were located in an intron of *KCNQ1*, and the association of this gene with diabetes was confirmatory.[15] To validate the other seven loci for the association with type 2 diabetes, we analyzed them in two independent replication panels of Japanese and Han-Chinese individuals (Table 1, Supplementary Table 2). Only one SNP, rs2250402, which is located in *EIF2AK4*, was found to be significantly associated in the replication-Japanese panel (*P*=0.039, OR=1.17, 95% CI=1.01–1.36). However, neither this SNP (*P*=0.41, OR=1.05) nor any of the other six SNPs showed such an association in the replication-Chinese panel. Meta-analyses for these SNPs showed that rs2307027 in *KRT4* and rs3785233 in *A2BP1* yielded *P*-values of <0.05 and ORs between 1.12 and 1.13 (Table 1). When the original second and third screening